NExT-OMNI: Towards Any-to-Any Omnimodal Foundation Models with Discrete Flow Matching

Anonymous authors
Paper under double-blind review

Abstract

Next-generation multimodal foundation models capable of any-to-any cross-modal generation and multi-turn interaction will serve as core components of artificial general intelligence systems, playing a pivotal role in human-machine interaction. However, most existing multimodal models remain constrained by autoregressive architectures, whose inherent limitations prevent a balanced integration of understanding and generation capabilities. Although hybrid and decoupling strategies have been explored to address these tasks within unified frameworks separately, their redundant, non-integrated designs limit their applicability to broader scenarios, such as cross-modal retrieval. In this work, we introduce NExT-OMNI, an open-source omnimodal foundation model that achieves unified modeling through discrete flow paradigms. By leveraging metric-induced probability paths and kinetic optimal velocities, NExT-OMNI natively supports any-to-any understanding and generation with enhanced response efficiency, while enabling broader application scenarios through concise unified representations rather than task-decoupled designs. Trained on large-scale interleaved text, image, video, and audio data, NExT-OMNI delivers competitive performance on multimodal understanding and generation benchmarks, while outperforming prior unified models in multi-turn multimodal interaction and cross-modal retrieval, highlighting its architectural advantages as a next-generation multimodal foundation model. To advance further research, we will release training details, data protocols, and open-source both the code and model checkpoints.

1 Introduction

Unified multimodal understanding and generation has emerged as a critical bottleneck for achieving artificial general intelligence (AGI), attracting growing academic attention (Dong et al., 2024; Ge et al., 2024; Fu et al., 2024; Xie & Wu, 2024). Numerous studies (Wu et al., 2024c; Dong et al., 2024; Ge et al., 2024; Wu et al., 2024b) have attempted to leverage successful autoregressive (AR) techniques from large language models (LLMs) (Touvron et al., 2023; Yang et al., 2024; Wu et al., 2024d) to achieve unified modeling of multimodal understanding and generation. However, these attempts have failed to achieve desired outcomes due to inherent conflicts within AR paradigms when handling understanding and generation tasks (Wu et al., 2024b;c; Dong et al., 2024).

Subsequent works have adopted hybrid architectures (Xie et al., 2024; Zhou et al., 2024) and modular decoupling techniques (Wu et al., 2024a; Deng et al., 2025; Chen et al., 2025a) to separately process understanding and generation tasks within relatively unified frameworks. These methods improve performance on both task categories and narrow the gap between open-source models and closed-source systems (OpenAI, 2025; DeepMind, 2025). Nevertheless, such AR-based hybrid architectures primarily rely on decoupling rather than fusion design. Although effective in understanding and generation tasks, they inevitably introduce additional parameterized modules, thereby increasing structural complexity and slowing inference. Moreover, this separated design struggles to support tasks that demand deep multimodal feature fusion and flexible any-to-any cross-modal tasks, such as cross-modal retrieval, which limits their applicability to more general multimodal scenarios.

In recent years, models based on discrete diffusion and flow matching have demonstrated competitive advantages over traditional AR counterparts across multiple domains, including language mod-

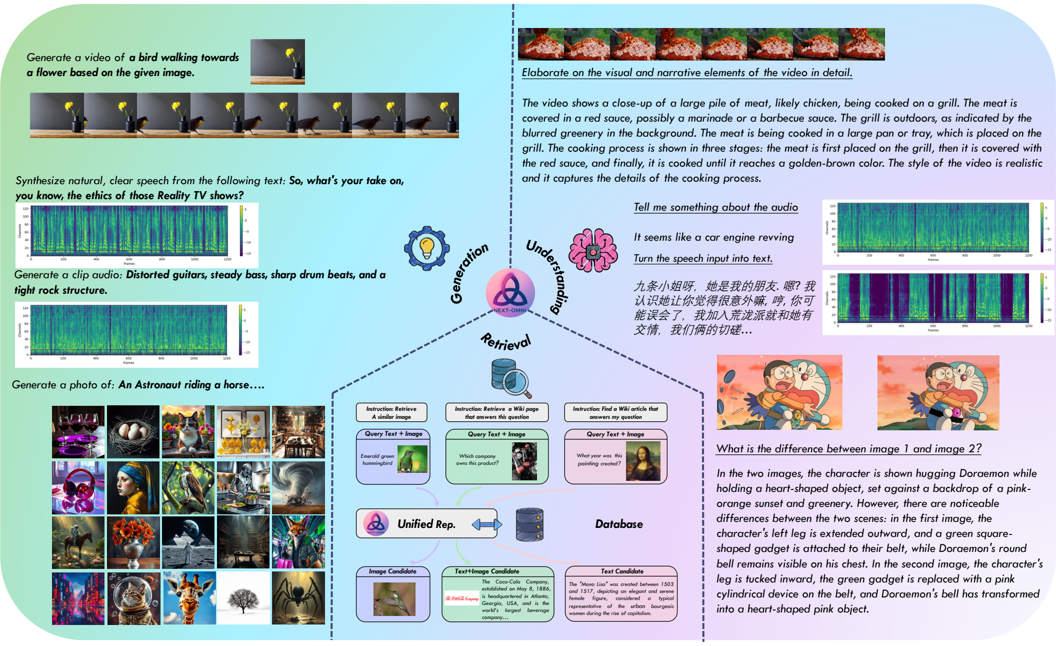

Generate a video of **a bird walking towards a flower based on the given image.**

Synthesize natural, clear speech from the following text: **So, what's your take on, you know, the ethics of those Reality TV shows?**

Generate a clip audio: **Distorted guitars, steady bass, sharp drum beats, and a tight rock structure.**

Generate a photo of: **An Astronaut riding a horse….**

Elaborate on the visual and narrative elements of the video in detail.

The video shows a close-up of a large pile of meat, likely chicken, being cooked on a grill. The meat is covered in a red sauce, possibly a marinade or a barbecue sauce. The grill is outdoors, as indicated by the blurred greenery in the background. The meat is being cooked in a large pan or tray, which is placed on the grill. The cooking process is shown in three stages: the meat is first placed on the grill, then it is covered with the red sauce, and finally, it is cooked until it reaches a golden-brown color. The style of the video is realistic and it captures the details of the cooking process.

Tell me something about the audio

It seems like a car engine revving

Turn the speech input into text.

九条小姐呀，她是我的朋友. 嗯? 我认识她让你觉得很意外嘛, 哼, 你可能误会了，我加入荒泷派就和她有交情，我们俩的切磋…

What is the difference between image 1 and image 2?

In the two images, the character is shown hugging Doraemon while holding a heart-shaped object, set against a backdrop of a pink-orange sunset and greenery. However, there are noticeable differences between the two scenes: in the first image, the character's left leg is extended outward, and a green square-shaped gadget is attached to their belt, while Doraemon's round bell remains visible on his chest. In the second image, the character's leg is tucked inward, the green gadget is replaced with a pink cylindrical device on the belt, and Doraemon's bell has transformed into a heart-shaped pink object.

Instruction: Retrieve A similar image

Query Text + Image: Emerald green hummingbird

Instruction: Retrieve a Wiki page that answers this question

Query Text + Image: Which company owns this product?

Instruction: Find a Wiki article that answers my question

Query Text + Image: What year was this painting created?

Image Candidate

Text+Image Candidate: The Coca-Cola Company, established on May 8, 1886, is headquartered in Atlanta, Georgia, USA, and is the world's largest beverage company…

Text Candidate: The "Mona Lisa" was created between 1503 and 1517, depicting an elegant and serene female figure, considered a typical representative of the urban bourgeois women during the rise of capitalism.

Figure 1: **Overview of the NExT-OMNI framework.** NExT-OMNI is a unified framework for omnimodal tasks, offering strong understanding, generation, and retrieval capabilities. The framework enables any-to-any operations across modalities for both generation and understanding tasks, while achieving accelerated processing. It also supports cross-modal retrieval by leveraging rich multimodal representations aggregated within its architecture.

eling (Nie et al., 2025; Ye et al., 2025a), image modeling (Rombach et al., 2022a; Li et al., 2024e), and audio modeling (Du et al., 2024; Li et al., 2025c). Unlike sequential AR models, these models begin with completely corrupted sequences and iteratively denoise entire sequences in parallel, enabling richer bidirectional information integration to enhance task performance. In addition, they achieve flexible and controllable generation through inherent iterative refinement processes, while demonstrating accelerated sampling potential through parallel decoding, providing a more promising fusion perspective for any-to-any multimodal understanding and generation tasks. However, this research direction remains underexplored, with its potential in unified understanding, generation, and retrieval yet to be fully realized.

To address this research gap, we propose NExT-OMNI, a fully open-source omnimodal foundation model based on discrete flow matching (DFM) techniques (Shaul et al., 2024), trained on large-scale, carefully curated interleaved multimodal datasets encompassing images, text, video, and audio. As shown in Figure 1, NExT-OMNI achieves faster any-to-any omnimodal generation through a streamlined unified architecture, while enabling more precise cross-modal retrieval through unified representations with intermediate feature fusion. Overall, NExT-OMNI not only demonstrates competitive performance with reduced latency on standard multimodal understanding and generation benchmarks, but also exhibits superior performance in multi-turn multimodal interaction and cross-modal retrieval. These results highlight that DFM-based unified multimodal understanding and generation modeling architectures provide a powerful fusion perspective for advancing multimodal unification with broader applicability.

The contributions of this paper are summarized as follows: 1) We propose NExT-OMNI, the first open-source omnimodal model built entirely on DFM, which is capable of achieving any-to-any generation across text, images, video, and audio with faster inference. 2) We design a reconstruction-enhanced unified representation with intermediate feature fusion. This design not only enables precise cross-modal retrieval but also supports multi-turn any-to-any multimodal interactions, demonstrating advantages over separated AR-based frameworks. 3) We conduct extensive experiments across understanding, generation, and retrieval benchmarks. Results show that NExT-OMNI consistently achieves competitive or superior performance with reduced latency, validating the potential of DFM-based architectures as a promising paradigm for unified multimodal modeling.

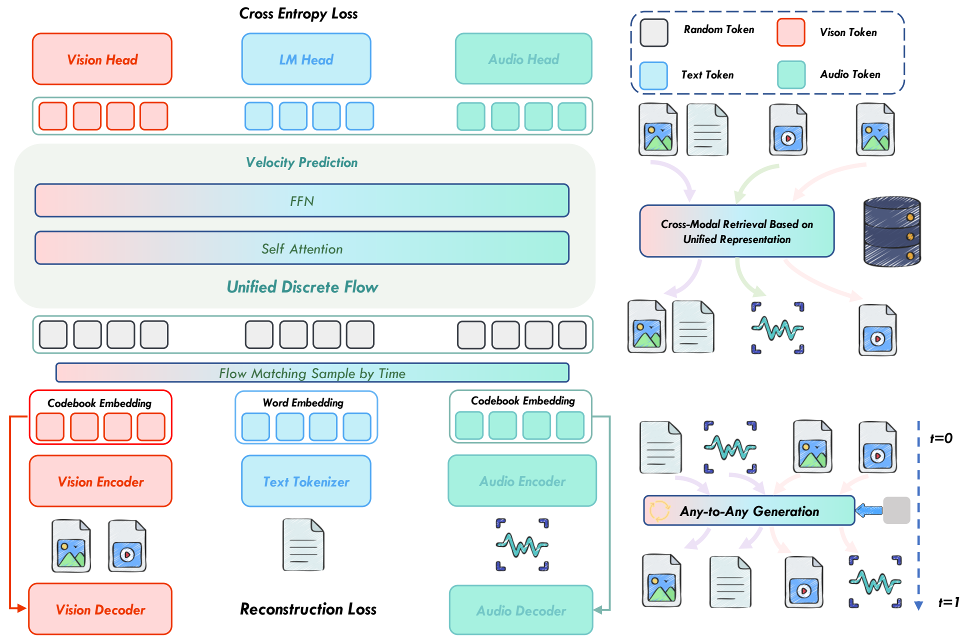

Figure 2: **Pipeline of the NExT-OMNI framework.** NExT-OMNI employs a DFM paradigm for unified omnimodal training, with multimodal self-attention at every layer to deeply fuse information across modalities. Unlike prior methods using multiple encoders or mixture-of-experts, it trains a single encoder simultaneously for understanding and generation, producing unified representations that enable any-to-any multimodal tasks with a streamlined architecture and strong generalization.

2 METHOD

2.1 ARCHITECTURE

Modality Encoders. We design vision and audio encoders grounded in unified representation principles (Luo et al., 2024a; Wu et al., 2024c; Ma et al., 2025a), enabling unified representational modeling. This design allows single-modal encoders to support both generation and understanding tasks, while also mitigating encoder redundancy.

Backbone. NExT-OMNI is initialized from the pretrained weights of AR-based LLMs and employs discrete flow matching within a three-stage progressive training framework on carefully curated omnimodal data. Following previous work (Gong et al., 2024b; Ye et al., 2025a; Wang et al., 2025), we retain the shifting operation to output logits by one position during training, enabling our model to inherit the next-token prediction capabilities of AR-based LLMs to the greatest extent possible. To expand model application scenarios such as cross-modal retrieval while streamlining model structure, we utilize deep bidirectional attention feature fusion rather than relying on additional MoE/MoT decoupling mechanisms (Xie et al., 2024; Deng et al., 2025).

Modality Heads. Since NExT-OMNI employs discrete flow matching, it eliminates the need for additional diffusion or flow heads (Dong et al., 2024; Luo et al., 2024a; Han et al., 2025; Chen et al., 2025a) specifically designed for generation optimization. Instead, it only requires lightweight heads for discrete token decoding, thereby substantially improving training efficiency and accelerating generation response. Furthermore, we introduce separate modality-specific heads for decoding each type of modality data, rather than extending the language model's vocabulary head directly. This design effectively preserves text generation capabilities. Additional details on the modality encoders and heads are provided in Appendix D.

2.2 UNIFIED REPRESENTATION MODELING

We first perform warmup training for unified representation modeling of the modality encoders. Two objectives are combined: (i) a reconstruction loss $\mathcal{L}_{\text{rec}}^{\text{M}}$, implemented with an auxiliary VQVAE (Van Den Oord et al., 2017) quantizer and modality-specific decoders that capture low-level details; (ii) a semantic alignment loss $\mathcal{L}_{\text{sem}}^{\text{M}}$ with an auxiliary text encoder or text decoder that emphasize high-level semantic alignments. Here, the superscript M corresponds to the modality. Given a continuous input vector z^{M}, which is obtained from a modality input X^{M} encoded by the corresponding modality encoder $\mathcal{E}^{\text{M}}$, the goal is to map it to the closest vector in a learnable codebook $\mathcal{C}^{\text{M}}$. The quantization process is formulated as $\mathrm{z}^{q} = \arg\min_{c \in \mathcal{C}^{\text{M}}} \|\mathrm{z}^{\text{M}} - c\|_2$, where $\mathcal{C}^{\text{M}} = \{c_1^{\text{M}}, c_2^{\text{M}}, \ldots, c_K^{\text{M}}\}$, and K is the number of codebook entries. The aim is to map the input z^{M} to the most representative vector $c_k^{\text{M}} \in \mathcal{C}^{\text{M}}$ via a VQ loss $\mathcal{L}_{\text{VQ}}^{\text{M}}$. Then we use the corresponding modality decoder $\mathcal{D}^{\text{M}}$ to restore the modality input X^{M} conditioned on the representative vector via a modality restoration loss $\mathcal{L}_{\text{R}}^{\text{M}}$. The reconstruction loss can be formulated as $\mathcal{L}_{\text{rec}}^{\text{M}} = \mathcal{L}_{\text{R}}^{\text{M}} + \mathcal{L}_{\text{VQ}}^{\text{M}} + \mathcal{L}_{\text{G}}^{\text{M}}$, where $\mathcal{L}_{\text{G}}^{\text{M}}$ is a discriminator loss. The total warmup training objective for our unified representation-based modality encoders can be expressed:

$$\mathcal{L}_{\text{total}}^{\text{M}} = \mathcal{L}_{\text{rec}}^{\text{M}} + \mathcal{L}_{\text{sem}}^{\text{M}}, \quad \text{M} \in \{\text{A}, \text{V}\}. \tag{1}$$

In more detail, to address the distinct semantic granularity requirements of vision modality V and audio modality A, we adopt token-level caption generation alignment $\mathcal{L}_{\text{sem}}^{\text{A}} = \mathcal{L}_{\text{cap}}^{\text{A}}$, for the audio encoder, following Whisper (Radford et al., 2023), and sentence-level contrastive semantic alignment $\mathcal{L}_{\text{sem}}^{\text{V}} = \mathcal{L}_{\text{constra}}^{\text{V}}$ for the vision encoder, following CLIP-ViT (Dosovitskiy et al., 2021).

2.3 Discrete Flow Matching Modeling

As illustrated in Figure 2, given an omnimodal vision-text-audio sequence input sampled from target distributions $q(\cdot)$, NExT-OMNI first utilizes VQVAE-based modality encoders and text tokenizers to convert it into discrete target token sequences $\mathrm{x}_1 = (\mathrm{x}_1^1, \mathrm{x}_1^2, \ldots, \mathrm{x}_1^D)$, where each element x_1^n is arranged in the order in which they appear in the original content. At each training step, a time $t \in [0, 1]$ is uniformly sampled, and a noisy sequence x_t is sampled according to the probability path $p_t(\cdot|\mathrm{x}_1)$ defined in Appendix A. Then, the model receives a noisy sequence x_t as an input and predicts x_1, outputting per-token logits for each position. Note that, unlike previous methods (Wang et al., 2024b; Han et al., 2025) that directly utilize discrete tokens, we extract continuous representative vector $c_{\mathrm{z}^q}^{\text{M}}$ with rich semantic and detailed information from the corresponding quantizer codebooks $\mathcal{C}^{\text{M}}$ of modality encoders based on discrete tokens, and achieve dimensional alignment with text embeddings through lightweight projection. This simple yet effective method enables the model to achieve superior performance in subsequent optimization. During training, we only perform correction training on the response portions of instruction data. The discrete flow matching (DFM) modeling is defined as the expected cross-entropy loss between the ground-truth sequence x_1 and the model's predicted distribution as follows:

$$\mathcal{L}_{\text{ce}} = \mathbb{E}_{t \sim \mathcal{U}[0,1],\, \mathrm{x}_1 \sim q(\cdot),\, \mathrm{x}_t \sim p_t(\cdot|\mathrm{x}_1)} \left[-\sum_{i=1}^{D} \log p_{1|t}\left(\mathrm{x}_1^i | \mathrm{x}_t\right) \right] \tag{2}$$

In addition to the cross-entropy loss mentioned above, to prevent the model from overly favoring semantic information during DFM training while discarding fine-grained information embedded in the unified representations of modality encoders, which would degrade model performance on understanding and generation tasks, we constrain the DFM training by reusing the corresponding reconstruction losses from the modality encoders in unified representation modeling. This maintains rich and detailed information, which not only improves understanding and generation performance but also enhances deep multimodal feature fusion, providing more precise cross-modal retrieval capabilities. The overall training objective can then be rewritten below:

$$\mathcal{L}_{\text{overall}} = \lambda_1 \cdot \mathcal{L}_{\text{ce}} + \lambda_2 \cdot \mathcal{L}_{\text{rec}}^{\text{V}} + \lambda_3 \cdot \mathcal{L}_{\text{rec}}^{\text{A}}, \tag{3}$$

where λ_1, λ_2, and λ_3 are the coefficient that controls the trade-offs between DFM modeling and the modality reconstruction loss. We adopt the GradNorm (Chen et al., 2018) method to dynamically adjust the coefficient, ensuring equal gradient update contributions to the model during training.

2.4 More Details of Training and Inference

During joint training, different data modalities require different training modules due to modality differences, and random mixed training leads to load imbalance that wastes substantial computational resources. To improve training efficiency, we conduct training for only one modality within any given training batch, achieving the joint training objective through interleaved training of multiple tasks and gradient accumulation, effectively enhancing computational resource utilization efficiency and achieving a 1.4× improvement in training efficiency.

As illustrated in Figure 3, to further improve NExT-OMNI's performance on understanding tasks, we design a dynamic length generation strategy. Specifically, during training, we insert additional <PAD> tokens to ensure that response sequences participating in training are multiples of the block size. During inference, leveraging the properties that simple tokens can be determined in a single denoising step, we dynamically adjust to appropriate preset generation lengths in block size increments based on <EOS> confidence, then perform multi-step iterative denoising. This strategy dramatically enhances the model's text generation capabilities at minimal cost. Furthermore, we observe phenomena similar to DLLM (Liu et al., 2025b) during the multi-step denoising process in inference, where most features change minimally throughout the multi-step denoising procedure, providing opportunities for inference acceleration using caching mechanisms. We cache and perform minimal updates on the instruction portion throughout the entire inference process, while adaptively updating during the response process based on the cosine similarity between value features and cached features. This vanilla adaptive cache implementation, combined with the parallel decoding advantages of NExT-OMNI's DFM architecture, achieves a 1.2× inference response speed improvement compared to AR architectures. Our cache acceleration and dynamic generation strategies enable superior performance with faster response speed.

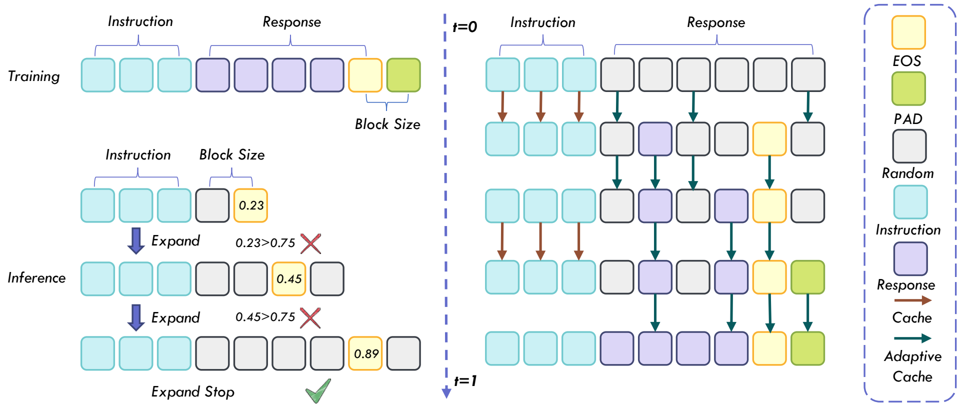

Figure 3: **Illustrations of dynamic generation strategy (left) and vanilla adaptive cache design (right).** During training, responses are padded to multiples of the block size, allowing the model to extend preset response lengths in block-size increments during inference. This improves performance on understanding tasks that require dynamic-length generation. The vanilla adaptive cache caches instruction features and selectively caches response features based on feature cosine similarity, accelerating inference and decoding. Combined with parallel decoding, this simple yet efficient caching design enables NExT-OMNI to generate responses faster than AR-based models.

3 Experiments

In this section, extensive experiments are conducted to demonstrate the superiority of the proposed NExT-OMNI and justify our claims. We first introduce implementation details (Section 3.1). Following this, a series of results on various practical tasks and subsequent discussions are provided, including omnimodal understanding (Section 3.2), vision interaction (Section 3.4), speech interaction (Section 3.3), and multimodal retrieval (Section 3.5). Finally, the ablation study (Section 3.6) is presented to examine the contributions of different components in NExT-OMNI, offering deeper insights into the factors that drive its success. For experiments on single-turn interactions such as text-to-image and text-to-audio generation, please refer to Appendix H for more details.

3.1 Implementation Details

Model Configurations. We initialize our vision encoder and audio encoder with CLIP-ViT-Large (Dosovitskiy et al., 2021) and Whisper-Turbo (Radford et al., 2023) weights, respectively, then perform joint training for reconstruction and semantic alignment using auxiliary VQVAE (Van Den Oord et al., 2017) and corresponding decoders. Specifically, we conduct warmup training on 70M image-text pairs constructed from LAION (Schuhmann et al., 2022) and DataComp (Li et al., 2024c). The image resolution is set to 256×256 with a downsampling rate of 16. We reuse the text encoder from CLIP-ViT to extract caption semantics for the computation of the contrastive loss $\mathcal{L}^{\text{V}}_{\text{constra}}$. For the audio encoder, we conduct warmup training using a combination of open-source datasets, including LibriSpeech (Panayotov et al., 2015), WenetSpeech (Zhang et al., 2022), and AudioCaps (Kim et al., 2019), totaling 2,000 hours, supplemented by proprietary speech and music datasets amounting to 100,000 hours. During this process, we set the maximum audio clip length to 15 seconds and employ Qwen2.5-0.5B (Yang et al., 2024) for the computation of the audio caption loss $\mathcal{L}^{\text{A}}_{\text{cap}}$. We initialize NExT-OMNI with Qwen2.5-7B (Yang et al., 2024) weights, equipped with the warmup-trained vision encoder and audio encoder, along with lightweight modality heads containing nearly 128M parameters, and conduct progressive three-stage DFM training on carefully constructed omnimodal data. Throughout this process, we set the classifier-free guidance (Ho & Salimans, 2022) probability to 0.1 for multimodal generation tasks and the response padding block size to 64 for multimodal understanding tasks. We reuse the reconstruction terms $\mathcal{L}^{\text{A}}_{\text{rec}}$ and $\mathcal{L}^{\text{V}}_{\text{rec}}$ from the modal encoder warmup. These steps enhance multimodal generation, understanding, and retrieval capabilities comprehensively.

Pre-Training (PT). To efficiently and stably conduct flow matching modeling, we perform omnimodal joint training during the alignment pre-training stage using short audio clips within 15 seconds, single images at 256×256 resolution with 16× downsampling, and short text with a maximum context window of 2K, leveraging large amounts of low-quality data to rapidly achieve omnimodal alignment. We train on a mixture of image-text pairs and audio-text pairs. Specifically, ImageNet-1K (Deng et al., 2009), JourneyDB (Pan et al., 2023), LAION (Schuhmann et al., 2022), and FLUX (Labs, 2024) synthetic data for image generation; re-captioned image-text pairs from COYO (Byeon et al., 2022), CommonCrawl (Common Crawl, 2007), LAION (Schuhmann et al., 2022), and DataComp (Li et al., 2024c) for image understanding; LibriSpeech (Panayotov et al., 2015), WenetSpeech (Zhang et al., 2022), AudioCaps (Kim et al., 2019), and proprietary data for audio understanding and generation. To prevent degradation of the model's textual capabilities, we sample shorter pure text data from Infinity-Instruct (Li et al., 2025a) and Evol-Instruct (Xu et al., 2024), and incorporate them into the mixed training dataset.

Continued Pre-Training (CPT). During the CPT stage, we increase image resolution to 384×384 and introduce long text, interleaved image-text, video, and long audio data with a maximum context window of 16K. This enables the model to support natural multi-turn visual and audio interactions while possessing the capability to understand and preliminarily generate short videos. For video data, we uniformly extract 8 frames as a multi-image input. For long audio data, we decompose them into multiple chunks with a maximum length of 15 seconds. Our experiments demonstrate that this simple strategy efficiently endows the model with video and long audio understanding and generation capabilities. Beyond partial resampling of pre-training stage data, we also incorporate PixMo (Deitke et al., 2024) and LLaVA-OneVision (Li et al., 2024a) training data for image understanding; FLUX (Labs, 2024) synthetic data for image generation; MMC4-Core (Zhu et al., 2023), OmniCorpus (Li et al., 2025b), and ShareGPT4Video (Chen et al., 2024c) supporting multi-image and short video understanding; OpenVid (Nan et al., 2024) and internal video data for video generation; OpenOmni (Luo et al., 2025) synthetic data exceeding 15 seconds and proprietary audio data for audio understanding and generation.

Supervised Fine-Tuning (SFT). In the SFT stage, we train the model to learn all multimodal-related instruction data, equipping it with any-to-any generation capabilities to accomplish diverse multimodal generation and understanding tasks. We collect LLaVA-OneVision (Li et al., 2024a) and PixMo (Deitke et al., 2024) instruction data for image generation; LLaVA-Video (Zhang et al., 2025b) instruction data for video understanding; OpenOmni (Luo et al., 2025) for multi-turn audio interaction; InterSyn (Ma et al., 2025b) for multi-turn image interaction; along with BLIP3-o (Chen et al., 2025a), ShareGPT-4o-Image (Chen et al., 2025b), Nano-consistent (Ye et al., 2025b) image generation, and TIP-I2V (Wang & Yang, 2024) video generation to construct an omnimodal training dataset. To further enhance the model's understanding, reasoning, and generation reasoning capabilities, we obtain 4M high-quality reasoning capability enhancement data through MMEvol (Luo et al., 2024b) sampling and filtering, and synthesize 5M reasoning-generated image data based on

Table 1: **Comparison with existing state-of-the-art omnimodal models on omnimodal understanding benchmarks, including OmniBench, WorldSense, and AV-Odyssey.** Here, "T", "V", and "A" represent text, vision, and audio modality inputs, respectively. We mark the best performance in **bold**.

Model	OmniBench			WorldSense			AV-Odyssey	AVG.
	T+V	T+A	T+A+V	A	T+A	T+A+V	T+A+V	
AnyGPT (Zhan et al., 2024)	20.1	16.2	18.0	16.5	17.2	16.2	-	-
OmniFlow (Li et al., 2025c)	20.4	18.7	20.6	20.4	18.9	19.7	-	-
Video-SALMONN (Sun et al., 2024a)	34.9	35.9	35.6	-	-	-	25.3	-
UnifiedIO2-large (Lu et al., 2024)	29.1	29.1	27.1	25.2	20.9	23.3	26.0	25.8
UnifiedIO2-xlarge (Lu et al., 2024)	34.8	31.2	38.0	23.4	20.7	24.7	26.3	28.4
UnifiedIO2-xxlarge (Lu et al., 2024)	33.5	32.5	34.0	25.9	23.7	25.9	27.2	29.0
NExT-GPT (Wu et al., 2023)	22.1	21.4	24.3	23.2	27.4	23.3	25.5	23.9
OneLLM (Han et al., 2024)	32.3	28.7	30.5	23.0	28.6	22.8	27.4	27.6
VideoLLaMA2 (Cheng et al., 2024)	31.7	26.2	28.9	23.8	28.5	25.4	26.8	27.3
VITA (Fu et al., 2024)	33.5	30.1	33.1	30.5	32.1	31.2	26.4	31.0
VITA 1.5 (Fu et al., 2025)	34.7	31.2	33.4	32.9	37.5	36.9	30.6	33.9
OpenOmni (Luo et al., 2025)	38.3	36.7	37.4	34.1	38.9	37.2	32.8	36.5
NExT-OMNI	**41.4**	**39.5**	**40.7**	**37.2**	**42.1**	**40.5**	**36.4**	**39.7**

FLUX (Labs, 2024) for image generation improvement. Based on high-quality instruction finetuning data, NExT-OMNI achieves superior performance across multiple evaluation benchmarks.

3.2 Omnimodal Understanding

To assess the omnimodal capabilities of NExT-OMNI, we conduct evaluations against current state-of-the-art omnimodal large language models (OLLMs) across three canonical benchmarks, including OmniBench (Li et al., 2024d), WorldSense (Hong et al., 2025), and AV-Odyssey (Gong et al., 2024a). As shown in Table 1, NExT-OMNI exhibits superior or comparable performance relative to advanced autoregressive-based OLLMs under various modal combination input conditions. In comparison with OpenOmni, our model achieves a 3.2 absolute average performance improvement across the three datasets. These results indicate that discrete flow matching (DFM) demonstrates potential as a viable alternative to the autoregressive (AR) paradigm for omnimodal modeling.

3.3 Speech Interaction

To verify NExT-OMNI's capabilities in multi-turn speech interaction, we conduct experiments on knowledge-based LLaMA Question and Web Question, covering both speech-to-text (S→T) and speech-to-speech (S→S) tasks. As shown in Table 2, under training with multi-turn speech instruction data of a similar scale, compared to AR-based speech-language models such as Stream-Omni (Zhang et al., 2025a), NExT-OMNI demonstrates competitive knowledge-based speech interaction capabilities on Spoken QA. This indicates that DFM-based omnimodal models can handle complex scenarios of multi-turn speech interaction, providing strong support for unified omnimodal generation and understanding tasks based on DFM.

Table 2: **Comparison with existing state-of-the-art unified speech-language model on multi-turn speech interaction benchmarks Spoken QA.** Here, "T" and "S" represent text and speech (belonging to the audio modality) inputs, respectively. We mark the best performance in **bold** and the second-best performance with an underline.

Model	Llama Q.		Web Q.		AVG.	
	S→T	S→S	S→T	S→S	S→T	S→S
SpeechGPT (Zhang et al., 2023a)	21.6	-	6.5	-	14.1	-
Moshi (Défossez et al., 2024)	62.3	21.0	26.6	9.2	44.5	15.1
GLM-4-Voice (Zeng et al., 2024)	64.7	50.7	32.2	15.9	48.5	33.3
Freeze-Omni (Wang et al., 2024c)	72.0	-	44.7	-	58.4	-
LLaMA-Omni (Fang et al., 2024)	67.7	49.0	33.4	23.7	50.6	36.4
VITA-1.5 (Fu et al., 2025)	76.7	-	42.7	-	59.7	-
Stream-Omni (Zhang et al., 2025a)	76.3	65.0	44.2	27.5	60.3	46.3
OpenOmni (Luo et al., 2025)	74.6	**67.2**	44.5	**28.9**	59.6	**48.1**
NExT-OMNI	**78.4**	66.4	**45.6**	28.3	**62.0**	47.4

3.4 Vision Interaction

To explore the high-level capabilities of NExT-OMNI in multi-turn vision interaction, we evaluate it on the interleaved image-text generation benchmark OpenING (Zhou et al., 2025). This benchmark requires models to perform multi-turn interleaved image generation based on input content and employs additional judge models for content consistency scoring, challenging the model's ability to naturally determine image generation positions and contextual understanding capabilities. As

Table 3: **Comparison with existing state-of-the-art unified vision-language model on multi-turn vision interaction benchmarks OpenING.** We mark the best performance in **bold**.

Model	GPT Evaluation				IntJudge Evaluation				AVG.
	FDT	w/o Tie	w/ Tie (0)	w/ Tie (.5)	FDT	w/o Tie	w/ Tie (0)	w/ Tie (.5)	
MiniGPT-5 (Zheng et al., 2023)	28.6	28.4	28.0	28.7	24.5	15.5	9.9	27.9	23.9
NExT-GPT (Wu et al., 2023)	22.6	22.4	22.1	22.7	31.0	21.7	13.4	32.6	23.5
DEEM (Luo et al., 2024a)	25.6	25.4	25.2	25.9	31.2	21.3	13.6	32.3	25.1
Show-o (Xie et al., 2024)	30.8	30.2	29.6	30.6	31.5	21.1	12.5	32.9	27.4
Emu2 (Sun et al., 2024b)	41.7	41.6	40.6	41.9	36.3	33.8	21.9	39.5	37.2
SEED-LLaMA (Ge et al., 2023b)	41.0	40.9	40.5	41.0	50.1	47.7	31.6	48.5	42.7
VILA-U (Wu et al., 2024c)	50.5	50.1	50.3	50.5	51.4	51.2	32.3	50.9	48.4
Anole (Chern et al., 2024)	53.4	53.1	52.6	53.1	53.4	52.0	33.9	51.3	50.4
SEED-X (Ge et al., 2024)	54.8	55.1	54.1	55.0	49.9	49.6	33.6	49.7	50.2
MMaDA (Yang et al., 2025)	51.4	52.6	51.1	52.5	47.6	47.2	31.8	47.4	47.7
FUDOKI (Wang et al., 2025)	47.6	49.2	47.8	48.6	44.4	44.1	30.1	44.2	44.5
NExT-OMNI	**58.7**	**58.3**	**57.4**	**58.6**	**56.3**	**57.7**	**37.5**	**55.4**	**55.0**

shown in Table 3, compared to vision-language unified models MMaDA (Yang et al., 2025) and FUDOKI (Wang et al., 2025) with similar architectures, NExT-OMNI demonstrates superior performance in multi-turn interactive generation for real-world usage scenarios, reflecting NExT-OMNI's advantages in general capabilities under multi-turn real-world contexts. Furthermore, compared to AR-based classical works VILA-U (Wu et al., 2024c) and SEED-X (Ge et al., 2024), NExT-OMNI also exhibits superior effectiveness, indicating that the DFM strategy possesses considerable potential in interactive generation consistency and merits further attention.

3.5 Multimodal Retrival

To provide more insights into the impact of paradigms and unified representations in broader multimodal task scenarios such as multimodal retrieval, we adopt the MM-Embed (Lin et al., 2024) approach to sample a 100K subset from the dataset M-BEIR (Wei et al., 2024) for multimodal retrieval training. Specifically, for input multimodal queries and retrieval candidates, we extract features from the <EOS> token after model encoding for multimodal retrieval ranking fine-tuning, and test on multiple multimodal retrieval benchmarks, including InfoSeek (Chen et al., 2023), OVEN (Hu et al., 2023), FashionIQ (Wu et al., 2021), and CIRR (Liu et al., 2021). We select classical works (Wu et al., 2024a; Deng et al., 2025; Wang et al., 2025; Wu et al., 2024c; Xie et al., 2024; Yang et al., 2025) with different paradigms and representations, and report Top 5 retrieval accuracy in Table 4.

We observe two phenomena. First, models based on discrete flow or diffusion (such as FUDOKI (Wang et al., 2025) and MMaDA (Yang et al., 2025)) outperform AR or hybrid architecture models (Wu et al., 2024a; Deng et al., 2025; Xie et al., 2024; Wu et al., 2024c). We attribute this to the fact that corrective bidirectional information encoding training methods can better aggregate contextual multimodal information compared to AR architectures based on causal masking mechanisms. During single feature extraction, they degrade to BERT-like feature extraction approaches (Lee et al., 2024), providing superior multimodal representations and demonstrating broader application potential of DFM. Another finding is that while using decoupling mechanisms (multiple encoders and MOT (Liang et al., 2024) mechanisms like Bagel) performs better on multimodal understanding and generation tasks, compared to unified representation methods (Wu et al., 2024c; Xie et al., 2024; Yang et al., 2025), they essentially involve routing between different models. The encoded features remain overly separated, making it difficult to produce unified representations, resulting in suboptimal performance on feature similarity-based multimodal retrieval tasks, which conversely limits the application scenarios of these methods. Based on these two findings, NExT-OMNI, which employs unified representation and DFM paradigm modeling, also demonstrates considerable potential in application scenarios beyond multimodal generation and understanding.

3.6 Ablation Study

We conduct ablation studies on key components of NExT-OMNI, including the modeling paradigm, representation methods, dynamic generation strategy (DGS), and reconstruction item. Benchmarks include image understanding (VQA^{v2} (Goyal et al., 2017)), audio understanding (Audio-

Table 4: **Comparison with existing classic unified models on various multimodal retrieval benchmarks, including InfoSeek, OVEN, FashionIQ, and CIRR.** Here, “T”, “A”, and “V” represent text, vision, and audio modality inputs, respectively. We mark the best performance in **bold**.

Model	Paradigm	Rep.	InfoSeek		OVEN		FashionIQ	CIRR	AVG.
			V+T→T	V+T→V+T	V+T→T	V+T→V+T	V+T→V	V+T→V	
Janus (Wu et al., 2024a)	AR	Decoupled	21.3	35.4	22.4	37.8	12.4	30.1	26.6
Bagel (Deng et al., 2025)	AR+Diff.	Decoupled	23.1	38.2	24.5	39.6	13.1	32.4	28.5
FUDOKI (Wang et al., 2025)	DFM	Decoupled	25.4	40.0	25.3	41.6	15.5	34.9	30.5
VILA-U (Wu et al., 2024c)	AR	Unified	23.3	37.4	24.0	38.5	13.6	33.8	28.4
Show-o (Xie et al., 2024)	AR+Discrete Diff.	Unified	24.8	39.3	25.6	42.5	15.9	35.2	30.6
MMaDA (Yang et al., 2025)	Discrete Diff.	Unified	25.9	40.8	26.5	43.7	17.5	36.3	31.8
NExT-OMNI	DFM	Unified	**27.6**	**41.5**	**27.1**	**44.6**	**18.9**	**37.6**	**32.9**

Table 5: **Ablation study on several key components of NExT-OMNI.** Here, “S” represents speech (belonging to the audio modality) inputs. We mark the best performance in **bold**.

Paradigm	Rep.	DGS.	Recon.	Und.		Gen.		Retrival		AVG.
				VQA^{v2}	AudioCaps	GenEval	Spoken QA (S→S)	InfoSeek	OVEN	
AR	**Decoupled**	×	×	55.2	62.8	53.4	16.4	28.3	32.1	41.4
DFM	**Decoupled**	×	×	52.3	60.1	59.8	20.3	29.6	33.7	42.6
DFM	**Unified**	×	×	51.7	59.4	59.2	19.5	32.8	35.6	43.0
DFM	**Unified**	✓	×	54.3	61.9	59.4	19.8	33.1	35.4	43.9
DFM	**Unified**	✓	✓	**56.2**	**63.4**	**62.6**	**21.7**	**33.7**	**36.1**	**45.6**

Caps (Kim et al., 2019)), image generation (GenEval (Ghosh et al., 2023)), speech generation (Spoken QA (Fang et al., 2024)), and multimodal retrieval (InfoSeek and OVEN).

Compared to the AR-based baseline with decoupled representations (i.e., an understanding-oriented encoder and a generation-oriented encoder), replacing the training paradigm with DFM (see Table 5) leads to a decline in understanding performance, but yields notable improvements in generation and retrieval tasks. When shifting further to unified representations, conflicts emerge due to the different granularity requirements of generation and understanding, resulting in an overall performance drop. Nevertheless, feature-based multimodal retrieval still benefits under this setting. These observations are consistent with our earlier findings, suggesting that unified representations may hold greater potential for broader applications.

When we introduce the DGS during training to better serve text generation tasks requiring dynamic length generation capabilities, we can significantly improve the performance on multimodal understanding tasks, achieving competitive performance with AR models. When we incorporate modality reconstruction loss terms during training, the model’s performance on generation and retrieval tasks is significantly enhanced, while also providing some gains for understanding tasks. This indicates that reconstruction can add more low-level fine-grained information constraints to features encoded by visual encoders, alleviating the model’s bias toward excessive focus on high-level semantic information, thereby enhancing fine-grained information in unified representations and providing good support for subsequent generation and retrieval tasks.

4 Conclusion

In this paper, we introduce NExT-OMNI, the first omnimodal foundation model fully built on discrete flow matching, which supports understanding, generation, and retrieval across text, images, video, and audio within a unified architecture. By incorporating reconstruction-feedback-enhanced unified representations and dynamic-length generation strategies, NExT-OMNI achieves deep fusion of multimodal features while substantially reducing model complexity. This design not only strengthens generation, understanding, and retrieval capabilities, but also establishes a new paradigm for unified multimodal modeling. Extensive experiments demonstrate the effectiveness of NExT-OMNI and provide insights into how architectural design interacts with unified representations in multimodal tasks. Looking ahead, we plan to extend NExT-OMNI to broader domains, such as action trajectory generation in vision-language-action models and video generation for physical AI understanding in world models, where we expect it to play an even greater role.

Ethics Statement

This work advances unified omnimodal large language models by introducing discrete flow matching modeling paradigms and reconstruction-enhanced unified representations, enhancing multimodal understanding, generation, and retrieval capabilities, enabling efficient text-vision-audio integration for applications such as assistive tools, creative content, and education. However, high-quality image and audio generation also poses risks, including potential misuse for misinformation or manipulation. While our model is not identity-specific, downstream applications should include safeguards such as watermarking and prompt filtering. We advocate for ethical use, emphasizing fairness, robustness, and transparency.

Reproducibility Statement

Experimental settings are carefully described and listed in Section 3. We detail the model design, data curation, and supplement implementation details in Appendix D, Appendix E, and Appendix F, respectively. To further ensure reproducibility, we promise to release training details, data protocols, and open-source both the code and model checkpoints.

References

Joshua Ainslie, James Lee-Thorp, Michiel De Jong, Yury Zemlyanskiy, Federico Lebrón, and Sumit Sanghai. Gqa: Training generalized multi-query transformer models from multi-head checkpoints. *arXiv preprint arXiv:2305.13245*, 2023.

Junyi Ao, Rui Wang, Long Zhou, Chengyi Wang, Shuo Ren, Yu Wu, Shujie Liu, Tom Ko, Qing Li, Yu Zhang, et al. Speecht5: Unified-modal encoder-decoder pre-training for spoken language processing. *arXiv preprint arXiv:2110.07205*, 2021.

Jinze Bai, Shuai Bai, Shusheng Yang, Shijie Wang, Sinan Tan, Peng Wang, Junyang Lin, Chang Zhou, and Jingren Zhou. Qwen-vl: A frontier large vision-language model with versatile abilities. *arXiv preprint arXiv:2308.12966*, 2023.

Shuai Bai, Keqin Chen, Xuejing Liu, Jialin Wang, Wenbin Ge, Sibo Song, Kai Dang, Peng Wang, Shijie Wang, Jun Tang, Humen Zhong, Yuanzhi Zhu, Mingkun Yang, Zhaohai Li, Jianqiang Wan, Pengfei Wang, Wei Ding, Zheren Fu, Yiheng Xu, Jiabo Ye, Xi Zhang, Tianbao Xie, Zesen Cheng, Hang Zhang, Zhibo Yang, Haiyang Xu, and Junyang Lin. Qwen2.5-vl technical report. *arXiv preprint arXiv:2502.13923*, 2025.

James Betker, Gabriel Goh, Li Jing, Tim Brooks, Jianfeng Wang, Linjie Li, Long Ouyang, Juntang Zhuang, Joyce Lee, Yufei Guo, et al. Improving image generation with better captions. *OpenAI blog*, 2023.

Minwoo Byeon, Beomhee Park, Haecheon Kim, Sungjun Lee, Woonhyuk Baek, and Saehoon Kim. Coyo-700m: Image-text pair dataset. https://github.com/kakaobrain/coyo-dataset, 2022.

Fabian Caba Heilbron, Victor Escorcia, Bernard Ghanem, and Juan Carlos Niebles. Activitynet: A large-scale video benchmark for human activity understanding. In *CVPR*, pp. 961–970, 2015.

David Chen and William B Dolan. Collecting highly parallel data for paraphrase evaluation. In *ACL*, pp. 190–200, 2011.

Jiuhai Chen, Zhiyang Xu, Xichen Pan, Yushi Hu, Can Qin, Tom Goldstein, Lifu Huang, Tianyi Zhou, Saining Xie, Silvio Savarese, et al. Blip3-o: A family of fully open unified multimodal models-architecture, training and dataset. *arXiv preprint arXiv:2505.09568*, 2025a.

Junsong Chen, Chongjian Ge, Enze Xie, Yue Wu, Lewei Yao, Xiaozhe Ren, Zhongdao Wang, Ping Luo, Huchuan Lu, and Zhenguo Li. Pixart-sigma: Weak-to-strong training of diffusion transformer for 4k text-to-image generation. In *ECCV*, 2024a.

Junying Chen, Zhenyang Cai, Pengcheng Chen, Shunian Chen, Ke Ji, Xidong Wang, Yunjin Yang, and Benyou Wang. Sharegpt-4o-image: Aligning multimodal models with gpt-4o-level image generation. *arXiv preprint arXiv:2506.18095*, 2025b.

Kai Chen, Yunhao Gou, Runhui Huang, Zhili Liu, Daxin Tan, Jing Xu, Chunwei Wang, Yi Zhu, Yihan Zeng, Kuo Yang, et al. Emova: Empowering language models to see, hear and speak with vivid emotions. *arXiv preprint arXiv:2409.18042*, 2024b.

Lin Chen, Jinsong Li, Xiaoyi Dong, Pan Zhang, Conghui He, Jiaqi Wang, Feng Zhao, and Dahua Lin. Sharegpt4v: Improving large multi-modal models with better captions. In *ECCV*, pp. 370–387, 2024c.

Xiaokang Chen, Chengyue Wu, Zhiyu Wu, Yiyang Ma, Xingchao Liu, Zizheng Pan, Wen Liu, Zhenda Xie, Xingkai Yu, Chong Ruan, and Ping Luo. Janus-pro: Unified multimodal understanding and generation with data and model scaling. *arXiv preprint arXiv:2501.17811*, 2025c.

Yang Chen, Hexiang Hu, Yi Luan, Haitian Sun, Soravit Changpinyo, Alan Ritter, and Ming-Wei Chang. Can pre-trained vision and language models answer visual information-seeking questions? *arXiv preprint arXiv:2302.11713*, 2023.

Zhao Chen, Vijay Badrinarayanan, Chen-Yu Lee, and Andrew Rabinovich. Gradnorm: Gradient normalization for adaptive loss balancing in deep multitask networks. In *ICML*, pp. 794–803, 2018.

Zesen Cheng, Sicong Leng, Hang Zhang, Yifei Xin, Xin Li, Guanzheng Chen, Yongxin Zhu, Wenqi Zhang, Ziyang Luo, Deli Zhao, et al. Videollama 2: Advancing spatial-temporal modeling and audio understanding in video-llms. *arXiv preprint arXiv:2406.07476*, 2024.

Ethan Chern, Jiadi Su, Yan Ma, and Pengfei Liu. Anole: An open, autoregressive, native large multimodal models for interleaved image-text generation. *arXiv preprint arxiv:2407.06135*, 2024.

Yunfei Chu, Jin Xu, Xiaohuan Zhou, Qian Yang, Shiliang Zhang, Zhijie Yan, Chang Zhou, and Jingren Zhou. Qwen-audio: Advancing universal audio understanding via unified large-scale audio-language models. *arXiv preprint arXiv:2311.07919*, 2023.

Common Crawl. Common crawl - open repository of web crawl data., 2007. URL https://commoncrawl.org/.

Wenliang Dai, Junnan Li, Dongxu Li, Anthony Tiong, Junqi Zhao, Weisheng Wang, Boyang Li, Pascale N Fung, and Steven Hoi. Instructblip: Towards general-purpose vision-language models with instruction tuning. In *NeurIPS*, pp. 49250–49267, 2023.

Google DeepMind. Gemini 2.0: Enhanced multimodal world models. https://blog.google/, 2025. Accessed: 2025-04-06.

Alexandre Défossez, Laurent Mazaré, Manu Orsini, Amélie Royer, Patrick Pérez, Hervé Jégou, Edouard Grave, and Neil Zeghidour. Moshi: a speech-text foundation model for real-time dialogue. *arXiv preprint arXiv:2410.00037*, 2024.

Matt Deitke, Christopher Clark, Sangho Lee, Rohun Tripathi, Yue Yang, Jae Sung Park, Mohammadreza Salehi, Niklas Muennighoff, Kyle Lo, Luca Soldaini, et al. Molmo and pixmo: Open weights and open data for state-of-the-art multimodal models. *arXiv e-prints*, pp. arXiv–2409, 2024.

Chaorui Deng, Deyao Zhu, Kunchang Li, Chenhui Gou, Feng Li, Zeyu Wang, Shu Zhong, Weihao Yu, Xiaonan Nie, Ziang Song, Guang Shi, and Haoqi Fan. Emerging properties in unified multimodal pretraining. *arXiv preprint arXiv:2505.14683*, 2025.

Jia Deng, Wei Dong, Richard Socher, Li-Jia Li, Kai Li, and Li Fei-Fei. Imagenet: A large-scale hierarchical image database. In *CVPR*, 2009.

Runpei Dong, Chunrui Han, Yuang Peng, Zekun Qi, Zheng Ge, Jinrong Yang, Liang Zhao, Jianjian Sun, Hongyu Zhou, Haoran Wei, et al. Dreamllm: Synergistic multimodal comprehension and creation. In *ICLR*, 2024.

Alexey Dosovitskiy, Lucas Beyer, Alexander Kolesnikov, Dirk Weissenborn, Xiaohua Zhai, Thomas Unterthiner, Mostafa Dehghani, Matthias Minderer, Georg Heigold, Sylvain Gelly, Jakob Uszkoreit, and Neil Houlsby. An image is worth 16x16 words: Transformers for image recognition at scale. In *ICLR*, 2021.

Zhihao Du, Qian Chen, Shiliang Zhang, Kai Hu, Heng Lu, Yexin Yang, Hangrui Hu, Siqi Zheng, Yue Gu, Ziyang Ma, et al. Cosyvoice: A scalable multilingual zero-shot text-to-speech synthesizer based on supervised semantic tokens. *arXiv preprint arXiv:2407.05407*, 2024.

Qingkai Fang, Shoutao Guo, Yan Zhou, Zhengrui Ma, Shaolei Zhang, and Yang Feng. Llama-omni: Seamless speech interaction with large language models. *arXiv preprint arXiv:2409.06666*, 2024.

Rongyao Fang, Aldrich Yu, Chengqi Duan, Linjiang Huang, Shuai Bai, Yuxuan Cai, Kun Wang, Si Liu, Xihui Liu, and Hongsheng Li. Flux-reason-6m & prism-bench: A million-scale text-to-image reasoning dataset and comprehensive benchmark. *arXiv preprint arXiv:2509.09680*, 2025.

Chaoyou Fu, Peixian Chen, Yunhang Shen, Yulei Qin, Mengdan Zhang, Xu Lin, Jinrui Yang, Xiawu Zheng, Ke Li, Xing Sun, et al. Mme: A comprehensive evaluation benchmark for multimodal large language models. *arXiv preprint arXiv:2306.13394*, 2023.

Chaoyou Fu, Haojia Lin, Zuwei Long, Yunhang Shen, Meng Zhao, Yifan Zhang, Xiong Wang, Di Yin, Long Ma, Xiawu Zheng, et al. Vita: Towards open-source interactive omni multimodal llm. *arXiv preprint arXiv:2408.05211*, 2024.

Chaoyou Fu, Haojia Lin, Xiong Wang, Yi-Fan Zhang, Yunhang Shen, Xiaoyu Liu, Haoyu Cao, Zuwei Long, Heting Gao, Ke Li, et al. Vita-1.5: Towards gpt-4o level real-time vision and speech interaction. *arXiv preprint arXiv:2501.01957*, 2025.

Yuying Ge, Yixiao Ge, Ziyun Zeng, Xintao Wang, and Ying Shan. Planting a seed of vision in large language model. *arXiv preprint arXiv:2307.08041*, 2023a.

Yuying Ge, Sijie Zhao, Ziyun Zeng, Yixiao Ge, Chen Li, Xintao Wang, and Ying Shan. Making llama see and draw with seed tokenizer. *arXiv preprint arXiv:2310.01218*, 2023b.

Yuying Ge, Sijie Zhao, Jinguo Zhu, Yixiao Ge, Kun Yi, Lin Song, Chen Li, Xiaohan Ding, and Ying Shan. Seed-x: Multimodal models with unified multi-granularity comprehension and generation. *arXiv preprint arxiv:2404.14396*, 2024.

Dhruba Ghosh, Hannaneh Hajishirzi, and Ludwig Schmidt. Geneval: An object-focused framework for evaluating text-to-image alignment. In *NeurIPS*, 2023.

Fabian Gloeckle, Badr Youbi Idrissi, Baptiste Rozière, David Lopez-Paz, and Gabriel Synnaeve. Better & faster large language models via multi-token prediction. *arXiv preprint arXiv:2404.19737*, 2024.

Kaixiong Gong, Kaituo Feng, Bohao Li, Yibing Wang, Mofan Cheng, Shijia Yang, Jiaming Han, Benyou Wang, Yutong Bai, Zhuoran Yang, et al. Av-odyssey bench: Can your multimodal llms really understand audio-visual information? *arXiv preprint arXiv:2412.02611*, 2024a.

Shansan Gong, Shivam Agarwal, Yizhe Zhang, Jiacheng Ye, Lin Zheng, Mukai Li, Chenxin An, Peilin Zhao, Wei Bi, Jiawei Han, et al. Scaling diffusion language models via adaptation from autoregressive models. *arXiv preprint arXiv:2410.17891*, 2024b.

Yash Goyal, Tejas Khot, Douglas Summers-Stay, Dhruv Batra, and Devi Parikh. Making the v in vqa matter: Elevating the role of image understanding in visual question answering. In *CVPR*, pp. 6904–6913, 2017.

Jarvis Guo, Tuney Zheng, Yuelin Bai, Bo Li, Yubo Wang, King Zhu, Yizhi Li, Graham Neubig, Wenhu Chen, and Xiang Yue. Mammoth-vl: Eliciting multimodal reasoning with instruction tuning at scale. *arXiv preprint arXiv:2412.05237*, 2024.

Jiaming Han, Kaixiong Gong, Yiyuan Zhang, Jiaqi Wang, Kaipeng Zhang, Dahua Lin, Yu Qiao, Peng Gao, and Xiangyu Yue. Onellm: One framework to align all modalities with language. In *CVPR*, pp. 26584–26595, 2024.

Jiaming Han, Hao Chen, Yang Zhao, Hanyu Wang, Qi Zhao, Ziyan Yang, Hao He, Xiangyu Yue, and Lu Jiang. Vision as a dialect: Unifying visual understanding and generation via text-aligned representations. *arXiv preprint arXiv:2506.18898*, 2025.

Jonathan Ho and Tim Salimans. Classifier-free diffusion guidance. *arXiv preprint arXiv:2207.12598*, 2022.

Jack Hong, Shilin Yan, Jiayin Cai, Xiaolong Jiang, Yao Hu, and Weidi Xie. Worldsense: Evaluating real-world omnimodal understanding for multimodal llms. *arXiv preprint arXiv:2502.04326*, 2025.

Wenyi Hong, Ming Ding, Wendi Zheng, Xinghan Liu, and Jie Tang. Cogvideo: Large-scale pretraining for text-to-video generation via transformers. *arXiv preprint arXiv:2205.15868*, 2022.

Hexiang Hu, Yi Luan, Yang Chen, Urvashi Khandelwal, Mandar Joshi, Kenton Lee, Kristina Toutanova, and Ming-Wei Chang. Open-domain visual entity recognition: Towards recognizing millions of wikipedia entities. In *ICCV*, pp. 12065–12075, 2023.

Xiwei Hu, Rui Wang, Yixiao Fang, Bin Fu, Pei Cheng, and Gang Yu. Ella: Equip diffusion models with llm for enhanced semantic alignment, 2024.

Ziqi Huang, Yinan He, Jiashuo Yu, Fan Zhang, Chenyang Si, Yuming Jiang, Yuanhan Zhang, Tianxing Wu, Qingyang Jin, Nattapol Chanpaisit, et al. Vbench: Comprehensive benchmark suite for video generative models. In *CVPR*, pp. 21807–21818, 2024.

IDEFICS. Introducing idefics: An open reproduction of state-of-the-art visual language model. https://huggingface.co/blog/idefics, 2023.

Shengpeng Ji, Ziyue Jiang, Wen Wang, Yifu Chen, Minghui Fang, Jialong Zuo, Qian Yang, Xize Cheng, Zehan Wang, Ruiqi Li, et al. Wavtokenizer: an efficient acoustic discrete codec tokenizer for audio language modeling. *arXiv preprint arXiv:2408.16532*, 2024.

Yang Jin, Kun Xu, Kun Xu, Liwei Chen, Chao Liao, Jianchao Tan, Quzhe Huang, Bin CHEN, Chengru Song, dai meng, Di ZHANG, Wenwu Ou, Kun Gai, and Yadong MU. Unified language-vision pretraining in LLM with dynamic discrete visual tokenization. In *ICLR*, 2024.

Tero Karras, Samuli Laine, and Timo Aila. A style-based generator architecture for generative adversarial networks. In *CVPR*, pp. 4401–4410, 2019.

Chris Dongjoo Kim, Byeongchang Kim, Hyunmin Lee, and Gunhee Kim. Audiocaps: Generating captions for audios in the wild. In *ACL*, pp. 119–132, 2019.

Black Forest Labs. Flux, 2024. URL https://github.com/black-forest-labs/flux.

Chankyu Lee, Rajarshi Roy, Mengyao Xu, Jonathan Raiman, Mohammad Shoeybi, Bryan Catanzaro, and Wei Ping. Nv-embed: Improved techniques for training llms as generalist embedding models. *arXiv preprint arXiv:2405.17428*, 2024.

Bo Li, Yuanhan Zhang, Dong Guo, Renrui Zhang, Feng Li, Hao Zhang, Kaichen Zhang, Peiyuan Zhang, Yanwei Li, Ziwei Liu, et al. Llava-onevision: Easy visual task transfer. *arXiv preprint arXiv:2408.03326*, 2024a.

Daiqing Li, Aleks Kamko, Ehsan Akhgari, Ali Sabet, Linmiao Xu, and Suhail Doshi. Playground v2. 5: Three insights towards enhancing aesthetic quality in text-to-image generation. *arXiv preprint arXiv:2402.17245*, 2024b.

Jijie Li, Li Du, Hanyu Zhao, Bo-wen Zhang, Liangdong Wang, Boyan Gao, Guang Liu, and Yonghua Lin. Infinity instruct: Scaling instruction selection and synthesis to enhance language models. *arXiv preprint arXiv:2506.11116*, 2025a.

KunChang Li, Yinan He, Yi Wang, Yizhuo Li, Wenhai Wang, Ping Luo, Yali Wang, Limin Wang, and Yu Qiao. Videochat: Chat-centric video understanding. *arXiv preprint arXiv:2305.06355*, 2023a.

Qingyun Li, Zhe Chen, Weiyun Wang, Wenhai Wang, Shenglong Ye, Zhenjiang Jin, et al. Omnicorpus: A unified multimodal corpus of 10 billion-level images interleaved with text. In *ICLR*, 2025b.

Shufan Li, Konstantinos Kallidromitis, Akash Gokul, Zichun Liao, Yusuke Kato, Kazuki Kozuka, and Aditya Grover. Omniflow: Any-to-any generation with multi-modal rectified flows. In *CVPR*, pp. 13178–13188, 2025c.

Xianhang Li, Haoqin Tu, Mude Hui, Zeyu Wang, Bingchen Zhao, Junfei Xiao, Sucheng Ren, Jieru Mei, Qing Liu, Huangjie Zheng, et al. What if we recaption billions of web images with llama-3? *arXiv preprint arXiv:2406.08478*, 2024c.

Yifan Li, Yifan Du, Kun Zhou, Jinpeng Wang, Wayne Xin Zhao, and Ji-Rong Wen. Evaluating object hallucination in large vision-language models. *arXiv preprint arXiv:2305.10355*, 2023b.

Yizhi Li, Ge Zhang, Yinghao Ma, Ruibin Yuan, Kang Zhu, Hangyu Guo, Yiming Liang, Jiaheng Liu, Jian Yang, Siwei Wu, et al. Omnibench: Towards the future of universal omni-language models. *arXiv preprint arXiv:2409.15272*, 2024d.

Yuncheng Li, Yale Song, Liangliang Cao, Joel Tetreault, Larry Goldberg, Alejandro Jaimes, and Jiebo Luo. Tgif: A new dataset and benchmark on animated gif description. In *CVPR*, pp. 4641–4650, 2016.

Zijie Li, Henry Li, Yichun Shi, Amir Barati Farimani, Yuval Kluger, Linjie Yang, and Peng Wang. Dual diffusion for unified image generation and understanding, 2024e. URL https://arxiv.org/abs/2501.00289.

Weixin Liang, Lili Yu, Liang Luo, Srinivasan Iyer, Ning Dong, Chunting Zhou, Gargi Ghosh, Mike Lewis, Wen-tau Yih, Luke Zettlemoyer, et al. Mixture-of-transformers: A sparse and scalable architecture for multi-modal foundation models. *arXiv preprint arXiv:2411.04996*, 2024.

Bin Lin, Yang Ye, Bin Zhu, Jiaxi Cui, Munan Ning, Peng Jin, and Li Yuan. Video-llava: Learning united visual representation by alignment before projection. *arXiv preprint arXiv:2311.10122*, 2023.

Sheng-Chieh Lin, Chankyu Lee, Mohammad Shoeybi, Jimmy Lin, Bryan Catanzaro, and Wei Ping. Mm-embed: Universal multimodal retrieval with multimodal llms. *arXiv preprint arXiv:2411.02571*, 2024.

Yaron Lipman, Ricky TQ Chen, Heli Ben-Hamu, Maximilian Nickel, and Matt Le. Flow matching for generative modeling. *arXiv preprint arXiv:2210.02747*, 2022.

Hao Liu, Wilson Yan, Matei Zaharia, and Pieter Abbeel. World model on million-length video and language with ringattention. *arXiv preprint arxiv:2402.08268*, 2024a.

Haotian Liu, Chunyuan Li, Yuheng Li, and Yong Jae Lee. Improved baselines with visual instruction tuning. *arXiv preprint arXiv:2310.03744*, 2023.

Haotian Liu, Chunyuan Li, Qingyang Wu, and Yong Jae Lee. Visual instruction tuning. In *NeurIPS*, 2024b.

Xiaohao Liu, Xiaobo Xia, Weixiang Zhao, Manyi Zhang, Xianzhi Yu, Xiu Su, Shuo Yang, See-Kiong Ng, and Tat-Seng Chua. L-mtp: Leap multi-token prediction beyond adjacent context for large language models. In *NeurIPS*, 2025a.

Yuan Liu, Haodong Duan, Yuanhan Zhang, Bo Li, Songyang Zhang, Wangbo Zhao, Yike Yuan, Jiaqi Wang, Conghui He, Ziwei Liu, et al. Mmbench: Is your multi-modal model an all-around player? In *ECCV*, 2024c.

Zheyuan Liu, Cristian Rodriguez-Opazo, Damien Teney, and Stephen Gould. Image retrieval on real-life images with pre-trained vision-and-language models. In *ICCV*, pp. 2125–2134, 2021.

Zhiyuan Liu, Yicun Yang, Yaojie Zhang, Junjie Chen, Chang Zou, Qingyuan Wei, Shaobo Wang, and Linfeng Zhang. dllm-cache: Accelerating diffusion large language models with adaptive caching. *arXiv preprint arXiv:2506.06295*, 2025b.

Jiasen Lu, Christopher Clark, Sangho Lee, Zichen Zhang, Savya Khosla, Ryan Marten, Derek Hoiem, and Aniruddha Kembhavi. Unified-io 2: Scaling autoregressive multimodal models with vision language audio and action. In *CVPR*, pp. 26439–26455, 2024.

Run Luo, Yunshui Li, Longze Chen, Wanwei He, Ting-En Lin, Ziqiang Liu, Lei Zhang, Zikai Song, Xiaobo Xia, Tongliang Liu, et al. Deem: Diffusion models serve as the eyes of large language models for image perception. *arXiv preprint arXiv:2405.15232*, 2024a.

Run Luo, Haonan Zhang, Longze Chen, Ting-En Lin, Xiong Liu, Yuchuan Wu, Min Yang, Minzheng Wang, Pengpeng Zeng, Lianli Gao, et al. Mmevol: Empowering multimodal large language models with evol-instruct. *arXiv preprint arXiv:2409.05840*, 2024b.

Run Luo, Ting-En Lin, Haonan Zhang, Yuchuan Wu, Xiong Liu, Min Yang, Yongbin Li, Longze Chen, Jiaming Li, Lei Zhang, et al. Openomni: Advancing open-source omnimodal large language models with progressive multimodal alignment and real-time self-aware emotional speech synthesis. *arXiv preprint arXiv:2501.04561*, 2025.

Chuofan Ma, Yi Jiang, Junfeng Wu, Jihan Yang, Xin Yu, Zehuan Yuan, Bingyue Peng, and Xiaojuan Qi. Unitok: A unified tokenizer for visual generation and understanding. *arXiv preprint arXiv:2502.20321*, 2025a.

Yiyi Ma, Yuanzhi Liang, Xiu Li, Chi Zhang, and Xuelong Li. Intersyn: Interleaved learning for dynamic motion synthesis in the wild. *arXiv preprint arXiv:2508.10297*, 2025b.

Muhammad Maaz, Hanoona Rasheed, Salman Khan, and Fahad Shahbaz Khan. Video-chatgpt: Towards detailed video understanding via large vision and language models. *arXiv preprint arXiv:2306.05424*, 2023.

Kepan Nan, Rui Xie, Penghao Zhou, Tiehan Fan, Zhenheng Yang, Zhijie Chen, Xiang Li, Jian Yang, and Ying Tai. Openvid-1m: A large-scale high-quality dataset for text-to-video generation. *arXiv preprint arXiv:2407.02371*, 2024.

Shen Nie, Fengqi Zhu, Zebin You, Xiaolu Zhang, Jingyang Ou, Jun Hu, Jun Zhou, Yankai Lin, Ji-Rong Wen, and Chongxuan Li. Large language diffusion models. *arXiv preprint arXiv:2502.09992*, 2025.

OpenAI. Sora: A data-driven physical engine for world modeling. https://openai.com/, 2025. Accessed: 2025-04-06.

Junting Pan, Keqiang Sun, Yuying Ge, Hao Li, Haodong Duan, Xiaoshi Wu, Renrui Zhang, Aojun Zhou, Zipeng Qin, Yi Wang, Jifeng Dai, Yu Qiao, and Hongsheng Li. Journeydb: A benchmark for generative image understanding, 2023.

Vassil Panayotov, Guoguo Chen, Daniel Povey, and Sanjeev Khudanpur. Librispeech: an asr corpus based on public domain audio books. In *ICASSP*, pp. 5206–5210, 2015.

Dustin Podell, Zion English, Kyle Lacey, Andreas Blattmann, Tim Dockhorn, Jonas Müller, Joe Penna, and Robin Rombach. Sdxl: Improving latent diffusion models for high-resolution image synthesis. *arXiv preprint arXiv:2307.01952*, 2023.

Liao Qu, Huichao Zhang, Yiheng Liu, Xu Wang, Yi Jiang, Yiming Gao, Hu Ye, Daniel K Du, Zehuan Yuan, and Xinglong Wu. Tokenflow: Unified image tokenizer for multimodal understanding and generation. *arXiv preprint arXiv:2412.03069*, 2024.

Alec Radford, Jong Wook Kim, Tao Xu, Greg Brockman, Christine McLeavey, and Ilya Sutskever. Robust speech recognition via large-scale weak supervision. In *ICML*, pp. 28492–28518, 2023.

Antony W Rix, John G Beerends, Michael P Hollier, and Andries P Hekstra. Perceptual evaluation of speech quality (pesq)-a new method for speech quality assessment of telephone networks and codecs. In *ICASSP*, pp. 749–752, 2001.

Robin Rombach, Andreas Blattmann, Dominik Lorenz, Patrick Esser, and Björn Ommer. High-resolution image synthesis with latent diffusion models. In *CVPR*, pp. 10684–10695, 2022a.

Robin Rombach, Andreas Blattmann, Dominik Lorenz, Patrick Esser, and Björn Ommer. High-resolution image synthesis with latent diffusion models. In *CVPR*, 2022b.

Takaaki Saeki, Detai Xin, Wataru Nakata, Tomoki Koriyama, Shinnosuke Takamichi, and Hiroshi Saruwatari. Utmos: Utokyo-sarulab system for voicemos challenge 2022. *arXiv preprint arXiv:2204.02152*, 2022.

Christoph Schuhmann, Romain Beaumont, Richard Vencu, Cade Gordon, Ross Wightman, Mehdi Cherti, Theo Coombes, Aarush Katta, Clayton Mullis, Mitchell Wortsman, et al. Laion-5b: An open large-scale dataset for training next generation image-text models. In *NeurIPS*, 2022.

Neta Shaul, Itai Gat, Marton Havasi, Daniel Severo, Anuroop Sriram, Peter Holderrieth, Brian Karrer, Yaron Lipman, and Ricky TQ Chen. Flow matching with general discrete paths: A kinetic-optimal perspective. *arXiv preprint arXiv:2412.03487*, 2024.

Guangzhi Sun, Wenyi Yu, Changli Tang, Xianzhao Chen, Tian Tan, Wei Li, Lu Lu, Zejun Ma, Yuxuan Wang, and Chao Zhang. video-salmonn: Speech-enhanced audio-visual large language models. *arXiv preprint arXiv:2406.15704*, 2024a.

Quan Sun, Qiying Yu, Yufeng Cui, Fan Zhang, Xiaosong Zhang, Yueze Wang, Hongcheng Gao, Jingjing Liu, Tiejun Huang, and Xinlong Wang. Emu: Generative pretraining in multimodality. In *ICLR*, 2023.

Quan Sun, Yufeng Cui, Xiaosong Zhang, Fan Zhang, Qiying Yu, Yueze Wang, Yongming Rao, Jingjing Liu, Tiejun Huang, and Xinlong Wang. Generative multimodal models are in-context learners. In *CVPR*, 2024b.

Chameleon Team. Chameleon: Mixed-modal early-fusion foundation models. *arXiv preprint arXiv:2405.09818*, 2024.

Gemini Team, Rohan Anil, Sebastian Borgeaud, Jean-Baptiste Alayrac, Jiahui Yu, Radu Soricut, Johan Schalkwyk, Andrew M Dai, Anja Hauth, Katie Millican, et al. Gemini: a family of highly capable multimodal models. *arXiv preprint arxiv:2312.11805*, 2023.

Changyao Tian, Xizhou Zhu, Yuwen Xiong, Weiyun Wang, Zhe Chen, Wenhai Wang, Yuntao Chen, Lewei Lu, Tong Lu, Jie Zhou, et al. Mm-interleaved: Interleaved image-text generative modeling via multi-modal feature synchronizer. *arXiv preprint arxiv:2401.10208*, 2024.

Shengbang Tong, David Fan, Jiachen Zhu, Yunyang Xiong, Xinlei Chen, Koustuv Sinha, Michael Rabbat, Yann LeCun, Saining Xie, and Zhuang Liu. Metamorph: Multimodal understanding and generation via instruction tuning. *arXiv preprint arXiv:2412.14164*, 2024.

Hugo Touvron, Thibaut Lavril, Gautier Izacard, Xavier Martinet, Marie-Anne Lachaux, Timothée Lacroix, Baptiste Rozière, Naman Goyal, Eric Hambro, Faisal Azhar, et al. Llama: Open and efficient foundation language models. *arXiv preprint arxiv:2302.13971*, 2023.

Aaron Van Den Oord, Oriol Vinyals, et al. Neural discrete representation learning. In *NeurIPS*, 2017.

Team Wan, Ang Wang, Baole Ai, Bin Wen, Chaojie Mao, Chen-Wei Xie, Di Chen, Feiwu Yu, Haiming Zhao, Jianxiao Yang, et al. Wan: Open and advanced large-scale video generative models. *arXiv preprint arXiv:2503.20314*, 2025.

Chunwei Wang, Guansong Lu, Junwei Yang, Runhui Huang, Jianhua Han, Lu Hou, Wei Zhang, and Hang Xu. Illume: Illuminating your llms to see, draw, and self-enhance. *arXiv preprint arXiv:2412.06673*, 2024a.

Jin Wang, Yao Lai, Aoxue Li, Shifeng Zhang, Jiacheng Sun, Ning Kang, Chengyue Wu, Zhenguo Li, and Ping Luo. Fudoki: Discrete flow-based unified understanding and generation via kinetic-optimal velocities. *arXiv preprint arXiv:2505.20147*, 2025.

Wenhao Wang and Yi Yang. Tip-i2v: A million-scale real text and image prompt dataset for image-to-video generation. *arXiv preprint arXiv:2411.04709*, 2024.

Xinlong Wang, Xiaosong Zhang, Zhengxiong Luo, Quan Sun, Yufeng Cui, Jinsheng Wang, Fan Zhang, Yueze Wang, Zhen Li, Qiying Yu, et al. Emu3: Next-token prediction is all you need. *arXiv preprint arxiv:2409.18869*, 2024b.

Xiong Wang, Yangze Li, Chaoyou Fu, Lei Xie, Ke Li, Xing Sun, and Long Ma. Freeze-omni: A smart and low latency speech-to-speech dialogue model with frozen llm. *arXiv preprint arXiv:2411.00774*, 2024c.

Y. Wang, H. Zeng, X. Li, J. Yang, Y. Shen, and J. Lu. Videogpt: Video generation via learning to generate. In *ICML*, 2022.

Cong Wei, Yang Chen, Haonan Chen, Hexiang Hu, Ge Zhang, Jie Fu, Alan Ritter, and Wenhu Chen. Uniir: Training and benchmarking universal multimodal information retrievers. In *ECCV*, pp. 387–404, 2024.

Chengyue Wu, Xiaokang Chen, Zhiyu Wu, Yiyang Ma, Xingchao Liu, Zizheng Pan, Wen Liu, Zhenda Xie, Xingkai Yu, Chong Ruan, and Ping Luo. Janus: Decoupling visual encoding for unified multimodal understanding and generation. *arXiv preprint arXiv:2410.13848*, 2024a.

Hui Wu, Yupeng Gao, Xiaoxiao Guo, Ziad Al-Halah, Steven Rennie, Kristen Grauman, and Rogerio Feris. Fashion iq: A new dataset towards retrieving images by natural language feedback. In *CVPR*, pp. 11307–11317, 2021.

Junfeng Wu, Yi Jiang, Chuofan Ma, Yuliang Liu, Hengshuang Zhao, Zehuan Yuan, Song Bai, and Xiang Bai. Liquid: Language models are scalable multi-modal generators. *arXiv preprint arXiv:2412.04332*, 2024b.

Shengqiong Wu, Hao Fei, Leigang Qu, Wei Ji, and Tat-Seng Chua. Next-gpt: Any-to-any multimodal llm. *arXiv preprint arxiv:2309.05519*, 2023.

Size Wu, Wenwei Zhang, Lumin Xu, Sheng Jin, Zhonghua Wu, Qingyi Tao, Wentao Liu, Wei Li, and Chen Change Loy. Harmonizing visual representations for unified multimodal understanding and generation. 2025. URL https://arxiv.org/abs/2503.21979.

Yecheng Wu, Zhuoyang Zhang, Junyu Chen, Haotian Tang, Dacheng Li, Yunhao Fang, Ligeng Zhu, Enze Xie, Hongxu Yin, Li Yi, et al. Vila-u: a unified foundation model integrating visual understanding and generation. *arXiv preprint arXiv:2409.04429*, 2024c.

Zhiyu Wu, Xiaokang Chen, Zizheng Pan, Xingchao Liu, Wen Liu, Damai Dai, Huazuo Gao, Yiyang Ma, Chengyue Wu, Bingxuan Wang, et al. Deepseek-vl2: Mixture-of-experts vision-language models for advanced multimodal understanding. *arXiv preprint arXiv:2412.10302*, 2024d.

Enze Xie, Junsong Chen, Yuyang Zhao, Jincheng Yu, Ligeng Zhu, Chengyue Wu, Yujun Lin, Zhekai Zhang, Muyang Li, Junyu Chen, et al. Sana 1.5: Efficient scaling of training-time and inference-time compute in linear diffusion transformer. *arXiv preprint arXiv:2501.18427*, 2025.

Jinheng Xie, Weijia Mao, Zechen Bai, David Junhao Zhang, Weihao Wang, Kevin Qinghong Lin, Yuchao Gu, Zhijie Chen, Zhenheng Yang, and Mike Zheng Shou. Show-o: One single transformer to unify multimodal understanding and generation. *arXiv preprint arxiv:2408.12528*, 2024.

Zhifei Xie and Changqiao Wu. Mini-omni2: Towards open-source gpt-4o model with vision, speech and duplex. *arXiv preprint arXiv:2410.11190*, 2024.

Can Xu, Qingfeng Sun, Kai Zheng, Xiubo Geng, Pu Zhao, Jiazhan Feng, Chongyang Tao, Qingwei Lin, and Daxin Jiang. Wizardlm: Empowering large pre-trained language models to follow complex instructions. In *ICLR*, 2024.

Dejing Xu, Zhou Zhao, Jun Xiao, Fei Wu, Hanwang Zhang, Xiangnan He, and Yueting Zhuang. Video question answering via gradually refined attention over appearance and motion. In *ACM MM*, pp. 1645–1653, 2017.

Jin Xu, Zhifang Guo, Jinzheng He, Hangrui Hu, Ting He, Shuai Bai, Keqin Chen, Jialin Wang, Yang Fan, Kai Dang, et al. Qwen2. 5-omni technical report. *arXiv preprint arXiv:2503.20215*, 2025a.

Jin Xu, Zhifang Guo, Hangrui Hu, Yunfei Chu, Xiong Wang, Jinzheng He, Yuxuan Wang, Xian Shi, Ting He, Xinfa Zhu, et al. Qwen3-omni technical report. *arXiv preprint arXiv:2509.17765*, 2025b.

An Yang, Baosong Yang, Beichen Zhang, Binyuan Hui, Bo Zheng, Bowen Yu, Chengyuan Li, Dayiheng Liu, Fei Huang, Haoran Wei, Huan Lin, Jian Yang, Jianhong Tu, Jianwei Zhang, Jianxin Yang, Jiaxi Yang, Jingren Zhou, Junyang Lin, Kai Dang, Keming Lu, Keqin Bao, Kexin Yang, Le Yu, Mei Li, Mingfeng Xue, Pei Zhang, Qin Zhu, Rui Men, Runji Lin, Tianhao Li, Tingyu Xia, Xingzhang Ren, Xuancheng Ren, Yang Fan, Yang Su, Yichang Zhang, Yu Wan, Yuqiong Liu, Zeyu Cui, Zhenru Zhang, and Zihan Qiu. Qwen2.5 technical report. *arXiv preprint arXiv:2412.15115*, 2024.

Ling Yang, Ye Tian, Bowen Li, Xinchen Zhang, Ke Shen, Yunhai Tong, and Mengdi Wang. Mmada: Multimodal large diffusion language models. *arXiv preprint arXiv:2505.15809*, 2025.

Jiacheng Ye, Zhihui Xie, Lin Zheng, Jiahui Gao, Zirui Wu, Xin Jiang, Zhenguo Li, and Lingpeng Kong. Dream 7b: Diffusion large language models. *arXiv preprint arXiv:2508.15487*, 2025a.

Junyan Ye, Dongzhi Jiang, Zihao Wang, Leqi Zhu, Zhenghao Hu, Zilong Huang, Jun He, Zhiyuan Yan, Jinghua Yu, Hongsheng Li, Conghui He, and Weijia Li. Echo-4o: Harnessing the power of gpt-4o synthetic images for improved image generation. *https://arxiv.org/abs/2508.09987*, 2025b.

Zhen Ye, Xinfa Zhu, Chi-Min Chan, Xinsheng Wang, Xu Tan, Jiahe Lei, Yi Peng, Haohe Liu, Yizhu Jin, Zheqi Dai, et al. Llasa: Scaling train-time and inference-time compute for llama-based speech synthesis. *arXiv preprint arXiv:2502.04128*, 2025c.

Weihao Yu, Zhengyuan Yang, Linjie Li, Jianfeng Wang, Kevin Lin, Zicheng Liu, Xinchao Wang, and Lijuan Wang. Mm-vet: Evaluating large multimodal models for integrated capabilities. In *ICML*, 2024.

Xiang Yue, Yuansheng Ni, Kai Zhang, Tianyu Zheng, Ruoqi Liu, Ge Zhang, Samuel Stevens, Dongfu Jiang, Weiming Ren, Yuxuan Sun, et al. Mmmu: A massive multi-discipline multimodal understanding and reasoning benchmark for expert agi. In *CVPR*, pp. 9556–9567, 2024.

Aohan Zeng, Zhengxiao Du, Mingdao Liu, Kedong Wang, Shengmin Jiang, Lei Zhao, Yuxiao Dong, and Jie Tang. Glm-4-voice: Towards intelligent and human-like end-to-end spoken chatbot, 2024. URL https://arxiv.org/abs/2412.02612.

Jun Zhan, Junqi Dai, Jiasheng Ye, Yunhua Zhou, Dong Zhang, Zhigeng Liu, Xin Zhang, Ruibin Yuan, Ge Zhang, Linyang Li, et al. Anygpt: Unified multimodal llm with discrete sequence modeling. *arXiv preprint arxiv:2402.12226*, 2024.

Binbin Zhang, Hang Lv, Pengcheng Guo, Qijie Shao, Chao Yang, Lei Xie, Xin Xu, Hui Bu, Xiaoyu Chen, Chenchen Zeng, et al. Wenetspeech: A 10000+ hours multi-domain mandarin corpus for speech recognition. In *ICASSP*, pp. 6182–6186, 2022.

Dong Zhang, Shimin Li, Xin Zhang, Jun Zhan, Pengyu Wang, Yaqian Zhou, and Xipeng Qiu. Speechgpt: Empowering large language models with intrinsic cross-modal conversational abilities. In *Findings of EMNLP*, pp. 15757–15773, 2023a.

Hang Zhang, Xin Li, and Lidong Bing. Video-llama: An instruction-tuned audio-visual language model for video understanding. *arXiv preprint arXiv:2306.02858*, 2023b.

Richard Zhang, Phillip Isola, Alexei A Efros, Eli Shechtman, and Oliver Wang. The unreasonable effectiveness of deep features as a perceptual metric. In *CVPR*, pp. 586–595, 2018.

Shaolei Zhang, Shoutao Guo, Qingkai Fang, Yan Zhou, and Yang Feng. Stream-omni: Simultaneous multimodal interactions with large language-vision-speech model. *arXiv preprint arXiv:2506.13642*, 2025a.

Yuanhan Zhang, Jinming Wu, Wei Li, Bo Li, Zejun Ma, Ziwei Liu, and Chunyuan Li. Llava-video: Video instruction tuning with synthetic data. *Transactions on Machine Learning Research*, 2025b.

Kaizhi Zheng, Xuehai He, and Xin Eric Wang. Minigpt-5: Interleaved vision-and-language generation via generative vokens. *arXiv preprint arXiv:2310.02239*, 2023.

Chunting Zhou, Lili Yu, Arun Babu, Kushal Tirumala, Michihiro Yasunaga, Leonid Shamis, Jacob Kahn, Xuezhe Ma, Luke Zettlemoyer, and Omer Levy. Transfusion: Predict the next token and diffuse images with one multi-modal model. *arXiv preprint arxiv:2408.11039*, 2024.

Pengfei Zhou, Xiaopeng Peng, Jiajun Song, Chuanhao Li, Zhaopan Xu, Yue Yang, Ziyao Guo, Hao Zhang, Yuqi Lin, Yefei He, et al. Opening: A comprehensive benchmark for judging open-ended interleaved image-text generation. In *CVPR*, pp. 56–66, 2025.

Wanrong Zhu, Jack Hessel, Anas Awadalla, Samir Yitzhak Gadre, Jesse Dodge, Alex Fang, Youngjae Yu, Ludwig Schmidt, William Yang Wang, and Yejin Choi. Multimodal c4: An open, billion-scale corpus of images interleaved with text. In *NeurIPS*, pp. 8958–8974, 2023.

Appendix

A Preliminaries of Discrete Flow Matching

We provide a brief introduction to the mathematical processes of training and inference in discrete flow matching (DFM) (Shaul et al., 2024). Analogous to continuous flow matching (Lipman et al., 2022), DFM defines a family of time-dependent probability distributions $\{p_t(\mathrm{x})\}_{t\in[0,1]}$ that define a smooth transition, or probability paths, from a source distribution $p(\mathrm{x})$ to a target distribution $q(\mathrm{x})$. Here, $\mathrm{x} = \{\mathrm{x}^1, \mathrm{x}^2, \dots, \mathrm{x}^D\}$ lies in the discrete space $\mathcal{S} = \mathcal{T}^D$, where D denotes the number of discrete variables and $\mathcal{T} = [K] = \{1, 2, \dots, K\}$ represents the finite set of possible discrete values. Each $p_t(\mathrm{x})$ is constructed as $p_t(\mathrm{x}) = \sum_{\mathrm{x}_1\in\mathcal{S}} p_t(\mathrm{x}|\mathrm{x}_1)q(\mathrm{x}_1)$, where the conditional distribution is factorized across dimensions. Namely, $p_t(\mathrm{x}|\mathrm{x}_1) = \prod_{i=1}^{D} p_t(\mathrm{x}^i|\mathrm{x}_1^i)$. Note that each $p_t(\mathrm{x}^i|\mathrm{x}_1^i)$ defines a univariate interpolation between a base distribution $p(\mathrm{x}^i)$ and a one-hot distribution $\delta_{\mathrm{x}_1^i}(\mathrm{x}^i)$[1]. A common design for the interpolation is the mixture path, defined via a time-dependent scheduler $\kappa_t(\mathrm{x}_1^i) \in [0, 1]$, i.e.,

$$p_t(\mathrm{x}^i|\mathrm{x}_1^i) = (1 - \kappa_t(\mathrm{x}_1^i))p(\mathrm{x}^i) + \kappa_t(\mathrm{x}_1^i)\delta_{\mathrm{x}_1^i}(\mathrm{x}^i), \tag{4}$$

where $\kappa_0(\cdot) = 0$ and $\kappa_1(\cdot) = 1$. To obtain a more semantically meaningful transition path, we can adopt a metric-induced probability path as follows:

$$p_t(\mathrm{x}^i|\mathrm{x}_1^i) = \mathrm{Softmax}(-\beta_t d(\mathrm{x}^i, \mathrm{x}_1^i)), \tag{5}$$

where $d(\cdot, \cdot)$ is the cosine distance function between token embeddings, and $\beta_t \in [0, \infty]$ is a monotonic schedule.

After minimizing the kinetic energy (Shaul et al., 2024), the probability velocities can be formulated as follows:

$$u_t^i(\mathrm{x}^i, \mathrm{z}|\mathrm{x}_1) = p_t(\mathrm{x}^i|\mathrm{x}_1^i)\frac{\partial \beta_t}{\partial t} \max\left\{d(\mathrm{z}^i, \mathrm{x}_1^i) - d(\mathrm{x}^i, \mathrm{x}_1^i), 0\right\}. \tag{6}$$

Intuitively, for the i-th coordinate $\mathrm{z}^i \in \mathcal{T}$, this velocity ensures that probability mass flows from the state z^i to the state x^i only when x^i lies closer to x_1^i than z^i does, i.e., $d(\mathrm{x}^i, \mathrm{x}_1^i) < d(\mathrm{z}^i, \mathrm{x}_1^i)$. As a result, the flow monotonically progresses toward x_1^i.

During training, we sample x_t from $p_t(\mathrm{x}^i|\mathrm{x}_1^i)$ and feed it into the model to fit the target x_1. During inference, we employ an Euler solver for enhanced sampling robustness as recommended in (Shaul et al., 2024). This solver simulates the continuous-time Markov chain (CTMC) process $\{\mathrm{x}_t\}_{t\in[0,1]}$. Given that $\mathrm{x}_t \sim p_t$, the solver updates the i-th coordinate from time t to $t{+}h$ following the procedure below:

- Sample $\mathrm{x}_1^i \sim p_{1|t}^i(\cdot|\mathrm{x}_t)$ from our model;
- Compute the total conditional transition rate $\lambda^i = \sum_{\mathrm{x}^i\neq\mathrm{x}_t^i} u_t^i(\mathrm{x}^i, \mathrm{x}_t^i|\mathrm{x}_1^i)$ (see Eq. (6));
- Draw a uniform random variable $\mathrm{Z}_{\text{change}}^i \sim \mathcal{U}[0, 1]$;
- Sample x_{t+h}^i as follows: if $\mathrm{Z}_{\text{change}}^i \leq 1 - \exp\{-h\lambda^i\}$, sample x_{t+h}^i from $\frac{u_t^i(\cdot,\mathrm{x}_t^i|\mathrm{x}_1^i)}{\lambda^i}(1 - \delta_{\mathrm{x}_t^i}(\cdot))$; otherwise set $\mathrm{x}_{t+h}^i = \mathrm{x}_t^i$.

The procedure begins with completely corrupted sequences and iteratively denoises entire sequences in parallel, enabling richer bidirectional information integration to enhance final performance. We set $\beta_t = c\left(\frac{t}{1-t}\right)^a$ with $c = 3$ and $a = 0.9$, as suggested in (Shaul et al., 2024).

B Related Work

Unified Vision-Language Models. Unified vision-language models (Team, 2024; Dong et al., 2024; Tian et al., 2024; Luo et al., 2024a; Wu et al., 2024b) have attracted significant research attention due to their powerful multimodal understanding and generation capabilities. SEED and the Emu series (Ge et al., 2023b; 2024; Sun et al., 2023; 2024b; Wang et al., 2024b) adopt discrete autoregressive modeling approaches, unifying multimodal understanding and generation through next-token

[1] If $\mathrm{x}^i = \mathrm{x}_1^i$, $\delta_{\mathrm{x}_1^i}(\mathrm{x}^i)$=1; else, $\delta_{\mathrm{x}_1^i}(\mathrm{x}^i)$=0.

prediction paradigms. However, this coarse unification approach is susceptible to granularity mismatches between understanding and generation tasks, hindering further performance improvements. The Janus series models (Wu et al., 2024a; Chen et al., 2025c) decouple visual encoding for understanding and generation to address granularity mismatch issues, but introducing additional encoders limits flexibility. Subsequently, VILA-U (Wu et al., 2024c) and UniTok (Ma et al., 2025a) focus on constructing unified representations, using unified encoders to alleviate granularity conflicts between generation and understanding tasks, but still adhere to autoregressive modeling paradigms and lag behind specialized models (Rombach et al., 2022a; Xie et al., 2025) in generation tasks. Some works, such as BLIP-3o (Chen et al., 2025a), introduce additional diffusion-based specialized generation models for generation optimization to achieve impressive results, but further increase methodological complexity. To balance the effectiveness of generation and understanding tasks, some works attempt to use hybrid architectures. For instance, Show-o (Xie et al., 2024) and Transfusion (Zhou et al., 2024) integrate diffusion objectives into large language models for image generation, but this design breaks the autoregressive paradigm and complicates the unification of both tasks. Bagel (Deng et al., 2025) introduces MOT (Liang et al., 2024) architecture to successfully achieve excellent performance in both tasks within a relatively unified hybrid architecture, but the introduction of these decoupling mechanisms makes generation and understanding separate components, departing significantly from the ideal of a concise unified architecture. Some works (Yang et al., 2025; Wang et al., 2025) attempt to completely abandon autoregressive architectures, pursuing unified vision-language modeling from the perspective of discrete diffusion or flow matching, achieving considerable results. However, due to the lack of robust language foundation model support and engineering optimization, speed and effectiveness remain suboptimal.

Omnimodal Language Models. With the advancement of multimodal research, models are increasingly shifting toward unified frameworks that seamlessly integrate diverse input and output modalities. By tokenizing different data types into shared representations, models such as AnyGPT (Zhan et al., 2024) and Unified-IO2 (Lu et al., 2024) achieve seamless cross-modal task adaptability, enabling them to process audio, text, and images without requiring significant architectural modifications. OneLLM (Han et al., 2024) and NExT-GPT (Wu et al., 2023) enhance generation and understanding performance by unifying input spaces and introducing additional diffusion heads. Meanwhile, video-SALMONN (Sun et al., 2024a) enhances video understanding by incorporating fine-grained temporal modeling, improving the model's ability to interpret speech and actions within videos. To enhance human-computer interaction, the VITA series (Fu et al., 2024; 2025) introduces duplex communication schemes, enabling fluid and intuitive exchanges between users and AI models. EMOVA (Chen et al., 2024b) and OpenOmni (Luo et al., 2025) further extend the expressive capabilities of multimodal systems by integrating controllable emotional speech synthesis, providing more natural and engaging user interactions. The Qwen-Omni series (Xu et al., 2025a;b) further expanded the scale of training models and data, greatly enhancing the performance of the omni models. However, these works still rely on autoregressive architectures and additional large-scale continuous flow matching modeling heads for omnimodal modeling, while more unified and lightweight discrete flow matching and diffusion architectures remain unexplored. To address this gap, we propose NExT-OMNI in this work.

C Limitation and Discussion

Limitation. Due to resource constraints, we conduct training and validation only at the 7B parameter scale with 2T tokens. While NExT-OMNI provides insights into how discrete flow matching can better unify generation, understanding, and retrieval tasks, its full potential has not been demonstrated due to the lack of corresponding large language model foundation support. In the future, we hope to explore broader application scenarios, such as trajectory generation in vision-language-action models and world model exploration, where visual generation assists physical perception, to demonstrate the potential of NExT-OMNI.

Discussion. Here, we provide further discussion on the future of omnimodal unified models. Some argue that building unified models consumes substantial resources yet struggles to achieve performance comparable to generation-only and understanding-only models, questioning the necessity of constructing unified models. We address this concern as follows: unified models are built to achieve greater generalizability. In the future, unified omnimodal models will serve as a "world brain" to interact with the real world, with their general capabilities expected to be continuously

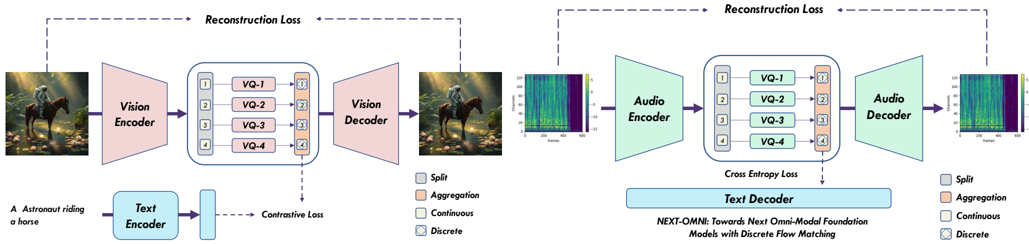

Figure 4: **The Pipeline of vision encoder (left) and audio encoder (right) warmup training.** During the modal encoder warmup training phase, self-supervised reconstruction is performed through additional quantizers and modal decoders, while semantic alignment at different granularities is achieved through text encoders or text decoders.

enhanced through multimodal data collected via interactions, thereby evolving iteratively to expand the model's capability boundaries and ultimately achieve Artificial General Intelligence (AGI). Our goal in building unified models is to enable mutual reinforcement among diverse tasks such as understanding and generation, ultimately expanding the boundaries of intelligence. For instance, through extensive vision generation learning, models can deepen their understanding of physical laws by precisely generating imagined moments, subsequently producing reasonable actions. Conversely, a deeper understanding of physical laws can enable models to generate more realistic image sequences. Based on this rationale, while building unified models may incur certain performance trade-offs, their general capabilities offer more promising prospects. On this spiraling path of development with its inevitable challenges, we must persist in this direction.

D Model Design

Here, we provide additional details regarding the design principles and training process of modality encoders and modality heads.

D.1 Modality Encoders

Similar to previous work (Luo et al., 2024a; Wu et al., 2024c; Ma et al., 2025a; Ye et al., 2025c; Wan et al., 2025), we design modality encoders based on unified representation methods, conducting simultaneous self-supervised reconstruction and semantic alignment optimization during the warmup training stage. As shown in Figure 4, we employ additional quantizers and modality decoders to assist reconstruction training, while utilizing text encoders and decoders for sentence-level and token-level semantic alignment training, respectively. To pursue superior performance, we adopt multi-codebook quantization (MCQ) (Ma et al., 2025a) for quantization, where separating the codebook into multiple independent sub-codebooks significantly enhances both reconstruction and semantic alignment effectiveness. However, we also observe that while increasing the number of sub-codebooks improves performance on reconstruction and downstream multimodal understanding tasks, it degrades performance on downstream multimodal generation tasks, as predicting multiple sub-codebook indices at a single position becomes more challenging. Therefore, to achieve an optimal trade-off, we set vocabulary sizes of 4×4096 and 2×2048 for the vision encoder and audio encoder in the warmup training, respectively.

Vision Encoder. We initialize our vision encoder with CLIP-ViT-Large (Dosovitskiy et al., 2021) weights and conduct unified representation training on nearly 70M image-text pairs composed of LAION (Schuhmann et al., 2022) and DataComp (Li et al., 2024c), incorporating both sentence-level image-text contrastive loss $\mathcal{L}_{\text{constra}}^{\text{V}}$ and VQVAE-based reconstruction loss $\mathcal{L}_{\text{rec}}^{\text{V}}$ optimization. In more detail, the VQVAE-based reconstruction loss consists of a pixel-level reconstruction loss $\mathcal{L}_{\text{R}}^{\text{V}}$, a perceptual loss $\mathcal{L}_{\text{P}}^{\text{V}}$ based on the LPIPS metric (Zhang et al., 2018), a discriminator loss $\mathcal{L}_{\text{G}}^{\text{V}}$ to enhance reconstruction fidelity (Karras et al., 2019), and a vector quantization loss $\mathcal{L}_{\text{VQ}}^{\text{V}}$ to minimize distance between the encoder output and its nearest code entry. It is denoted as $\mathcal{L}_{\text{rec}}^{\text{V}} = \mathcal{L}_{\text{R}}^{\text{V}} + \lambda_{\text{VQ}} \cdot \mathcal{L}_{\text{VQ}}^{\text{V}} + \lambda_{\text{P}} \cdot \mathcal{L}_{\text{P}}^{\text{V}} + \lambda_{\text{G}} \cdot \mathcal{L}_{\text{G}}^{\text{V}}$, where λ denotes the weight factor for the corresponding loss

Table 6: **Comparison with existing state-of-the-art vision tokenizer and audio tokenizer.** We mark the best performance in **bold**.

Model	Codebooks	UTMOS↑	PESQ↑	STOI↑	Model	Codebooks	rFID↓	Acc↑
WavTokenizer	4096	4.048	2.373	0.914	UniTok	8×4096	0.38	78.6
Audio Encoder (Ours)	2×2048	**4.126**	**2.467**	**0.923**	Vision Encoder (Ours)	4×4096	**0.33**	**79.4**

term. The image-text contrastive loss term $\mathcal{L}^{\mathrm{V}}_{\mathrm{constra}}$ is basically the same as in CLIP-VIT (Dosovitskiy et al., 2021). Therefore, the final loss term can be written as $\mathcal{L}^{\mathrm{V}}_{\mathrm{overall}} = \mathcal{L}^{\mathrm{V}}_{\mathrm{rec}} + \mathcal{L}^{\mathrm{V}}_{\mathrm{contra}}$. During this process, we maintain training hyperparameters consistent with UniTok (Ma et al., 2025a).

Audio Encoder. We initialize our audio encoder with Whisper-Turbo (Radford et al., 2023) weights and conduct unified representation training on nearly 102K hours of audio-text pairs composed of LibriSpeech (Panayotov et al., 2015), WeNetSpeech (Zhang et al., 2022), AudioCaps (Kim et al., 2019), and proprietary data, incorporating both token-level audio caption loss $\mathcal{L}^{\mathrm{A}}_{\mathrm{cap}}$ and VQVAE-based reconstruction loss $\mathcal{L}^{\mathrm{A}}_{\mathrm{rec}}$ optimization. The VQVAE-based reconstruction loss consists of a mel-spectrum reconstruction loss $\mathcal{L}^{\mathrm{A}}_{\mathrm{R}}$, a feature matching loss $\mathcal{L}^{\mathrm{A}}_{\mathrm{F}}$ based on a L2 norm loss, a discriminator loss $\mathcal{L}^{\mathrm{A}}_{\mathrm{G}}$ (Ji et al., 2024), and a vector quantization loss $\mathcal{L}^{\mathrm{A}}_{\mathrm{VQ}}$ to minimize distance between the encoder output and its nearest code entry. It is denoted as $\mathcal{L}^{\mathrm{A}}_{\mathrm{rec}} = \mathcal{L}^{\mathrm{A}}_{\mathrm{R}} + \lambda_{\mathrm{VQ}} \cdot \mathcal{L}^{\mathrm{A}}_{\mathrm{VQ}} + \lambda_{\mathrm{F}} \cdot \mathcal{L}^{A}_{\mathrm{F}} + \lambda_{\mathrm{G}} \cdot \mathcal{L}^{A}_{\mathrm{G}}$, where λ is the weight factor for the corresponding loss term. The audio-text caption loss term $\mathcal{L}^{\mathrm{A}}_{\mathrm{cap}}$ is basically the same as in Qwen-Audio (Chu et al., 2023). Therefore, the final loss term can be written as $\mathcal{L}^{\mathrm{A}}_{\mathrm{overall}} = \mathcal{L}^{\mathrm{A}}_{\mathrm{rec}} + \mathcal{L}^{\mathrm{A}}_{\mathrm{cap}}$. During this process, we maintain training hyperparameters consistent with WavTokenizer (Ji et al., 2024).

Quantitative and Qualitative Analysis. To validate the effectiveness of our warmup-trained vision encoder, we conduct image reconstruction and classification evaluation on ImageNet (Deng et al., 2009), reporting rFID (IDEFICS, 2023) and zero-shot classification accuracy, and compare with the state-of-the-art unified representation vision encoder UniTok (Ma et al., 2025a). Similar to the vision encoder configuration, we perform speech reconstruction comparison tests on the LibriSpeech test-clean split (Panayotov et al., 2015), employing UTMOS (Saeki et al., 2022), PESQ (Rix et al., 2001), and STOI (Ji et al., 2024) metrics, and compare with the state-of-the-art WavTokenizer (Wang et al., 2022). As shown in Table 6, our modality encoders demonstrate superior reconstruction and semantic classification performance, capable of producing reliable unified representations for multimodal generation, understanding, and retrieval. Furthermore, to more intuitively demonstrate the superiority of our modal encoders, we provide visualization results of reconstructions. As shown in Figure 6, we can observe that our vision encoder achieves better reconstruction performance compared to UniTokin details such as font edges and bear eye colors. As shown in Figure 5, we can see that our audio encoder produces clearer reconstructed mel-spectrograms for different audio types compared to WavTokenizer. These results validate the effectiveness of our modality encoder warmup training.

Table 7: **Ablation study on the scalability of NExT-OMNI.** Here, "S" represents speech (belonging to the audio modality) inputs. We mark the best performance in **bold**.

Model Size	Training Steps	Und.			Gen.			AVG.
		VQA$^{\text{v2}}$	AudioCaps	ActivityNet-QA	GenEval	Spoken QA (S→S)	VBench	
0.5B	0.5K	42.1	48.6	28.3	18.2	8.4	12.7	26.4
1.5B	0.5K	45.3	52.3	31.7	22.8	11.2	16.3	30.0
7B	0.5K	48.7	55.9	34.2	28.5	13.7	20.1	33.5
7B	1K	52.4	59.1	36.1	45.2	17.3	27.4	39.6
7B	1.5K	54.9	61.7	37.4	58.9	20.1	32.8	44.3
7B	2K	**56.2**	**63.4**	**37.8**	**62.6**	**21.7**	**34.6**	**46.1**

D.2 Modality Heads

Since we employ multi-codebook quantization (MCQ) for quantization, prediction requires forecasting multiple sub-codebook indices for a single position, which poses challenges for vision and audio head architectures. To overcome this problem, we design two different modality head structures, as illustrated in Figure 7. The left structure represents an autoregressive multi-sub-codebook

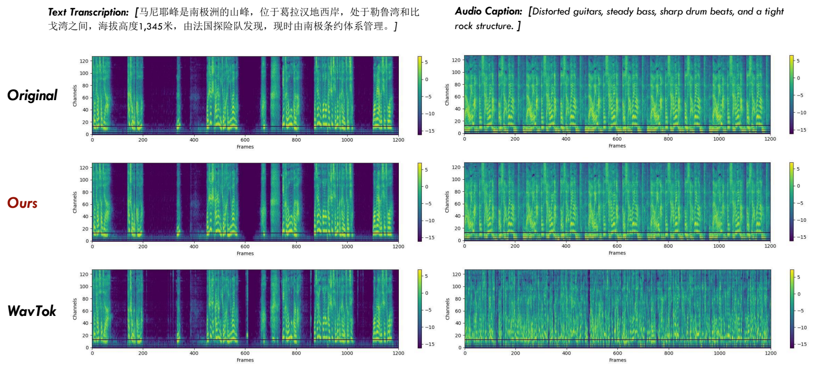

Figure 5: **Qualitative results on audio reconstruction in a max duration of 15s.**

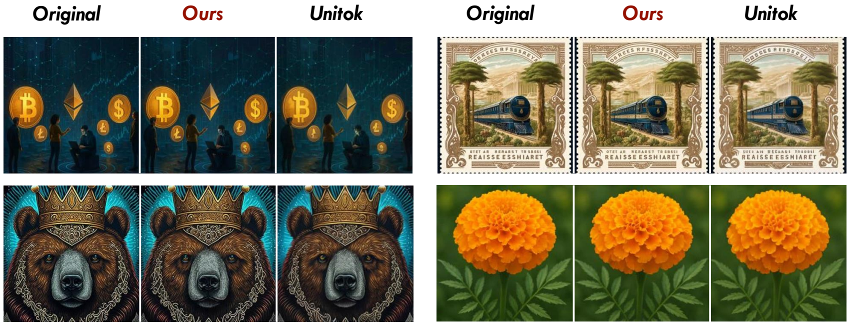

Figure 6: **Qualitative results on image reconstruction in a resolution of 256×256.**

index prediction modal head, which uses the hidden features output by NExT-OMNI at each position as conditions to complete the prediction of multiple sub-codebook indices through the next-token prediction paradigm. The right structure employs multiple separate heads to complete the prediction of multiple sub-codebook indices in parallel through multi-token prediction (Gloeckle et al., 2024; Liu et al., 2025a). Under equal parameter counts, the former provides more stable prediction results compared to the latter at the cost of slightly increased computational overhead, and is therefore adopted in our framework.

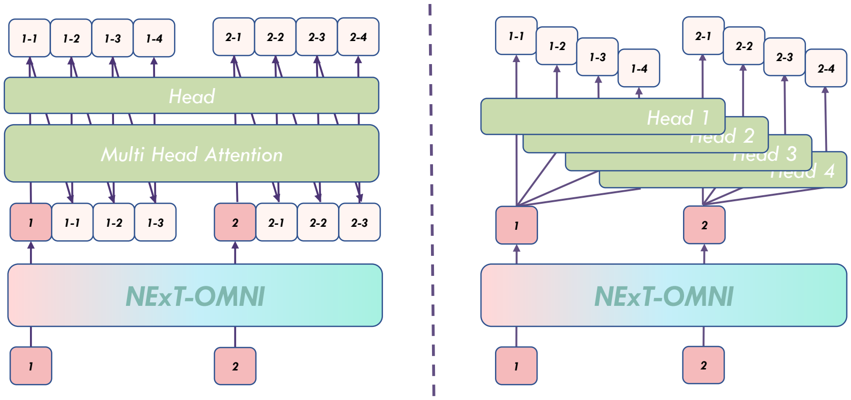

Figure 7: **Illustration of modality heads.** We design two different lightweight modal head structures for multiple sub-codebook indices prediction: next-token prediction (left) and multi-token prediction (right).

Table 8: **Overview of stages, training data, tasks, and sizes used for building NExT-OMNI**. Here, “I”, “T”, “A”, and “V” are the abbreviations of the image, text, audio, and vision, respectively.

Model	Stage	Data	Task	Size
Vision Encoder	Warmup	LAION (Schuhmann et al., 2022), DataComp (Li et al., 2024c),COYO (Byeon et al., 2022)	I→I, I→T	70M
Audio Encoder	Warmup	LibriSpeech (Panayotov et al., 2015), WenetSpeech (Zhang et al., 2022) AudioCaps (Kim et al., 2019), Proprietary Data	A→A, A→T	102K Hours
NExT-OMNI	PT	LLaVA-Recap-CC12M (Li et al., 2024a; Common Crawl, 2007), DataComp (Li et al., 2024c)	I→T	32M
		Blip3-o (Chen et al., 2025a), ImageNet-1K (Deng et al., 2009), JourneyDB (Pan et al., 2023)	T→I	25M
		Infinity-Instruct (Li et al., 2025a), Evol-Instruct (Xu et al., 2024)	Text	4M
		Proprietary Data, AudioCaps (Kim et al., 2019) LibriSpeech (Panayotov et al., 2015), WenetSpeech (Zhang et al., 2022)	A→T	16M
		Proprietary Data, AudioCaps (Kim et al., 2019)	T→A	6M
	CPT	LLaVA-O (Li et al., 2024a), PixMo (Deitke et al., 2024),MAmmoTH-VL (Guo et al., 2024)	I→T	10M
		Blip3-o (Chen et al., 2025a), Flux-Reason (Fang et al., 2025)	T→I	12M
		MMC4-core (Zhu et al., 2023), OmniCorpus (Li et al., 2025b) ShareGPT4Video (Chen et al., 2024c)	V→T	12M
		OpenVid (Nan et al., 2024), Internal Video Data	T→V	2M
		Infinity-Instruct (Li et al., 2025a), Evol-Instruct (Xu et al., 2024)	Text	2.3M
		Proprietary Data, AudioCaps (Kim et al., 2019)	A→T	12M
		OpenOmni (Luo et al., 2025), AudioCaps (Kim et al., 2019)	T→A	1.3M
	SFT	LLaVA-O (Li et al., 2024a), PixMo (Deitke et al., 2024), MMEvol (Luo et al., 2024b), Und-4M	I→T	7.6M
		OpenOmni (Luo et al., 2025)	T+A→T+A	0.5M
		InterSyn (Ma et al., 2025b)	T+I→T+I	1.7M
		Infinity-Instruct (Li et al., 2025a), Evol-Instruct (Xu et al., 2024)	Text	0.8M
		LLaVA-Video (Zhang et al., 2025b)	V→T	0.9M
		OpenVid (Nan et al., 2024), TIP-I2V (Wang & Yang, 2024)	T→V,T+I→V	1M
		BLIP3-o-60K (Chen et al., 2025a), ShareGPT-4o-Image (Chen et al., 2025b) Gen-5M, Nano-consistent (Ye et al., 2025b)	T→I, T+I→I	5.8M

E Data Curation

E.1 Dataset Curation Details

In addition to proprietary data, we collect publicly available data encompassing diverse tasks for three-stage progressive training, including generation-related tasks such as text-to-image, text-to-video, and text-to-audio, as well as understanding-related tasks, including image understanding, video understanding, and audio understanding. We summarize the important information of all training data in Table 8.

E.2 Dataset Synthetic Details

Visual Understanding. We randomly sample 1.2M data from LLaVA-OneVision (Li et al., 2024a) and PixMo (Deitke et al., 2024) datasets as seed data, and apply the MMEvol (Luo et al., 2024b) algorithm using the Qwen2.5-VL (Bai et al., 2025) model as the generator. Through three rounds of evolution, we construct approximately 4M instruction data (Und-4M) that are rich in diversity and complexity, to enhance the model’s capability for solving complex problems.

Image Generation. Based on user prompts from JourneyDB (Pan et al., 2023) and Midjourney-Prompts datasets, we use the Qwen2.5 (Yang et al., 2024) model to construct numerous similar synthetic prompts containing more fine-grained descriptions. Subsequently, we employ FLUX (Labs, 2024) as the image generator to rapidly generate large quantities of images based on user and synthetic prompts under the configuration of 4 sampling steps and 512×512 resolution. Finally, we collect approximately 5M high-quality synthetic data (Gen-5M).

F Additional Implementation Details

We report additional implementation details about training hyper-parameters and training data in Table 9.

Table 9: **Training recipes for NExT-OMNI.** The three training stages are introduced in Section 3.1. `Stage I`: Pre-Training (PT), `Stage II`: Continue Pre-Training (CPT), `Stage III`: Supervised Fine-tuning (SFT).

	`Stage I`	`Stage II`	`Stage III`
Phase	PT	CPT	SFT
		Training Hyper-Parameters	
Image Resolution	256×256	384×384	384×384
Audio Duration	$\leq$15s	$\geq$15s	$\geq$15s
Video Frames		$\leq$8	$\leq$8
LLM	Qwen2.5 7B	Qwen2.5 7B	Qwen2.5 7B
Learning Rate	2e-5 (modality encoder&decoder) 1e-4 (others)	1e-6 (modality encoder&decoder) 2e-5 (others)	1e-6 (modality encoder&decoder) 2e-5 (others)
Optimizer	AdamW	AdamW	AdamW
Optimizer hyper-parameters	$\beta_1, \beta_2, \epsilon$=0.9, 0.995, 1e-6	$\beta_1, \beta_2, \epsilon$=0.9, 0.999, 1e-8	$\beta_1, \beta_2, \epsilon$=0.9, 0.999, 1e-8
Weight Decay	0.05	0.05	0.05
Training iterations	10K	18K	25K
Warmup steps	1K	500	500
Learning Rate Scheduler	Cosine	Cosine	Cosine
Batch Size Per GPU	16	8	4
Maximum Token Length	2K	16K	16K
		Training Data	
Data Size	$\sim$83M	$\sim$52M	$\sim$18M
Data Type	Pair	Pair/Interleave	Instruction

G Additional Ablation Study

Although NExT-OMNI demonstrates competitive performance against the SOTA methods, its scalability has yet to be validated. As is well known, scalability is crucial for model performance. We conduct ablation experiments to assess the scalability concerning data count and model size. As shown in Table 7, gradually increasing the training data enables the model to successfully scale while achieving improved results. Additionally, increasing the sizes of backbone leads to sustained performance enhancements, indicating that NExT-OMNI possesses good scalability.

H Additional Experiments Results

Image Understanding. We evaluate the image understanding capabilities of NExT-OMNI on several benchmarks, including POPE (Li et al., 2023b), MME-P (Fu et al., 2023), SEED (Ge et al., 2023a), MMB (Liu et al., 2024c), GQA (Ainslie et al., 2023), MMMU (Yue et al., 2024), and MM-Vet (Yu et al., 2024). As shown in Table 3, NExT-OMNI not only outperforms models MMaDA and FUDOKI with similar architectures, but also achieves highly competitive results compared to autoregressive (AR)-based multimodal large language models. Notably, NExT-OMNI unleashes the potential of discrete flow matching (DFM) in understanding tasks through dynamic length generation and caching methods, while achieving faster generation speeds compared to AR models as shown in Figure 12. These results demonstrate that DFM represents a highly promising alternative to AR architectures and merits significant attention.

Image Generation. We evaluate the image generation capabilities of NExT-OMNI on the widely used GenEval (Ghosh et al., 2023) and DPG-Bench (Hu et al., 2024) benchmarks. NExT-OMNI achieves competitive overall performance in both Table 11 and Table 12, scoring 0.85 on GenEval and 84.46 on DPG-Bench, demonstrating strong performance in both generation-only and understanding-generation categories with smaller model parameters and faster response speeds. These results highlight the advantages of the discrete flow matching framework modeling, which allows bidirectional integration of visual information, first generating image layouts and then progressively filling in details, better aligning with the natural characteristics of image generation.

Audio Generation and Understanding. We validate our audio understanding and generation capabilities on benchmarks LibirSpeech (Panayotov et al., 2015) and AudioCaps (Kim et al., 2019). As shown in Table 13, compared to other omnimodal models, NExT-OMNI, as the first model to employ discrete flow matching modeling, achieves significantly superior performance in natural audio generation, understanding, speech translation, and speech synthesis. These results further validate the generalizability and scalability of discrete flow matching modeling, providing potential for future applications in protein molecular structure prediction, 3D model generation, and other domains.

Table 10: **Multimodal understanding performance on various benchmarks.** “Und.” and “Gen.” denote the abbreviations of “Understanding” and “Generation”. † denotes models that integrate an external pre-trained diffusion model.

Model	**Paradigm**	**# Params**	**POPE**	**MME-P**	**MMB**	**SEED**	**GQA**	**MMMU**	**MM-Vet**
Und. Only									
LLaVA (Liu et al., 2024b)	AR	7B	76.3	809.6	38.7	33.5	-	-	25.5
LLaVA-v1.5 (Liu et al., 2023)	AR	7B	85.9	1510.7	64.3	58.6	62.0	35.4	31.1
InstructBLIP (Dai et al., 2023)	AR	7B	-	-	36.0	53.4	49.2	-	26.2
Qwen-VL-Chat (Bai et al., 2023)	AR	7B	-	1487.5	60.6	58.2	57.5	-	-
IDEFICS-9B (IDEFICS, 2023)	AR	8B	-	-	48.2	-	38.4	-	-
Emu3-Chat (Wang et al., 2024b)	AR	8B	85.2	1244.0	58.5	68.2	60.3	31.6	37.2
InstructBLIP (Dai et al., 2023)	AR	13B	78.9	1212.8	-	-	49.5	-	25.6
Und. and Gen.									
LaVIT† (Jin et al., 2024)	AR	7B	-	-	-	-	46.8	-	-
MetaMorph† (Tong et al., 2024)	AR	8B	-	-	75.2	71.8	-	-	-
Gemini-Nano-1 (Team et al., 2023)	-	1.8B	-	-	-	-	-	26.3	-
ILLUME (Wang et al., 2024a)	AR	7B	88.5	1445.3	65.1	72.9	-	38.2	37.0
TokenFlow-XL (Qu et al., 2024)	AR	13B	86.8	1545.9	68.9	68.7	62.7	38.7	40.7
LWM (Liu et al., 2024a)	AR	7B	75.2	-	-	-	44.8	-	9.6
VILA-U (Wu et al., 2024c)	AR	7B	85.8	1401.8	-	59.0	60.8	-	33.5
Chameleon (Team, 2024)	AR	7B	-	-	-	-	-	22.4	8.3
Janus (Wu et al., 2024a)	AR	1.5B	87.0	1338.0	69.4	63.7	59.1	30.5	34.3
Janus-Pro (Chen et al., 2025c)	AR	1.5B	86.2	1444.0	75.5	68.3	59.3	36.3	39.8
Show-o (Xie et al., 2024)	AR+Discrete Diff.	1.3B	73.8	948.4	-	-	48.7	25.1	-
D-Dit (Li et al., 2024e)	Discrete Diff.+Diff.	2.0B	84.0	1124.7	-	-	59.2	-	-
FUDOKI (Wang et al., 2025)	DFM	1.5B	86.1	1485.4	73.9	68.2	57.6	34.3	38.0
MMaDA (Yang et al., 2025)	Discrete Diff.	8B	86.1	1410.7	68.5	64.2	61.3	30.2	-
NExT-OMNI	DFM	7B	87.4	1537.8	78.9	76.3	62.7	43.7	40.1

Table 11: **Visual Generation Results on GenEval (Ghosh et al., 2023).** “Und.” and “Gen.” denote the abbreviations of “Understanding” and “Generation”.

Model	**Paradigm**	**Single Obj.**	**Two Obj.**	**Counting**	**Colors**	**Position**	**Color Attri.**	**Overall↑**
Gen. Only								
SDv1.5 (Rombach et al., 2022a)	Diff.	0.97	0.38	0.35	0.76	0.04	0.06	0.43
PixArt-α (Chen et al., 2024a)	Diff.	0.98	0.50	0.44	0.80	0.08	0.07	0.48
SDv2.1 (Rombach et al., 2022a)	Diff.	0.98	0.51	0.44	0.85	0.07	0.17	0.50
Emu3-Gen (Wang et al., 2024b)	AR	0.98	0.71	0.34	0.81	0.17	0.21	0.54
SDXL (Podell et al., 2023)	Diff.	0.98	0.74	0.39	0.85	0.15	0.23	0.55
DALLE3 (Betker et al., 2023)	-	0.96	0.87	0.47	0.83	0.43	0.45	0.67
SD3-Medium (Rombach et al., 2022b)	Diff.	0.99	0.94	0.72	0.89	0.33	0.60	0.74
SANA-1.5 (Xie et al., 2025)	Diff.	0.99	0.93	0.86	0.84	0.59	0.65	0.81
Und. and Gen.								
Chameleon (Team, 2024)	AR	-	-	-	-	-	-	0.39
LWM (Liu et al., 2024a)	AR	0.93	0.41	0.46	0.79	0.09	0.15	0.47
SEED-X (Ge et al., 2024)	AR	0.97	0.58	0.26	0.80	0.19	0.14	0.49
Show-o (Xie et al., 2024)	AR+Discrete Diff.	0.95	0.52	0.49	0.82	0.11	0.28	0.53
Transfusion (Zhou et al., 2024)	AR+Diff.	-	-	-	-	-	-	0.63
D-DiT (Li et al., 2024e)	Discrete Diff.+Diff.	0.97	0.80	0.54	0.76	0.32	0.50	0.65
ILLUME (Wang et al., 2024a)	AR	0.99	0.86	0.45	0.71	0.39	0.28	0.61
Janus (Wu et al., 2024a)	AR	0.97	0.68	0.30	0.84	0.46	0.42	0.61
Harmon (Wu et al., 2025)	AR	0.99	0.86	0.66	0.85	0.74	0.48	0.76
Janus-Pro (Chen et al., 2025c)	AR	0.99	0.89	0.59	0.90	0.79	0.66	0.80
Tar (Han et al., 2025)	AR	0.99	0.91	0.76	0.81	0.57	0.51	0.76
MMaDA (Yang et al., 2025)	Discrete Diff.	0.99	0.76	0.61	0.84	0.20	0.37	0.63
FUDOKI (Wang et al., 2025)	DFM	0.96	0.85	0.56	0.88	0.68	0.67	0.77
NExT-OMNI	DFM	0.99	0.92	0.79	0.85	0.78	0.74	0.85

Video Understanding. We evaluate the video understanding capabilities of NExT-OMNI on several benchmarks, including MSVD-QA (Chen & Dolan, 2011), MSRVTT-QA (Xu et al., 2017),TGIF-QA (Li et al., 2016), and ActivityNet-QA (Caba Heilbron et al., 2015). As shown in Table 14, compared to models in understanding only or unified understanding-generation, NExT-OMNI achieves superior performance across all metrics, demonstrating that the DFM-based framework possesses considerable capability in understanding spatiotemporal relationships.

Video Generation. For video generation, we evaluate NExT-OMNI on VBench (Huang et al., 2024) and compare it against classical approaches, including Open-Sora (OpenAI, 2025), VILA-U (Wu et al., 2024c), and CogVideo (Hong et al., 2022). The results presented in Table 15 demonstrate that our method achieves superior performance compared to these autoregressive (AR)-based classical methods, highlighting the potential of discrete flow matching (DFM) in short video generation.

Table 12: **Visual Generation Results on DPG Bench (Hu et al., 2024).** “Und.” and “Gen.” denote the abbreviations of “Understanding” and “Generation”.

Model	Paradigm	Global	Entity	Attribute	Relation	Other	Overall↑
Gen. Only							
SDv1.5 (Rombach et al., 2022a)	Diff.	74.63	74.23	75.39	73.49	67.81	63.18
PixArt-α (Chen et al., 2024a)	Diff.	74.97	79.32	78.60	82.57	76.96	71.11
Emu3-Gen (Wang et al., 2024b)	AR	85.21	86.68	86.84	90.22	83.15	80.60
SDXL (Podell et al., 2023)	Diff.	83.27	82.43	80.91	86.76	80.41	74.65
Playground v2.5 (Li et al., 2024b)	-	83.06	82.59	81.20	84.08	83.50	75.47
PixArt-Σ (Chen et al., 2024a)	AR	86.89	82.89	88.94	86.59	87.68	80.54
DALLE3 (Betker et al., 2023)	Diff.	90.97	89.61	88.39	90.58	89.83	83.50
SD3-Medium (Rombach et al., 2022b)	Diff.	87.90	91.01	88.83	80.70	88.68	84.08
Und. and Gen.							
Show-o (Xie et al., 2024)	AR+Discrete Diff.	-	-	-	-	-	67.48
TokenFlow-XL (Qu et al., 2024)	AR	78.72	79.22	81.29	85.22	71.20	73.38
Janus (Wu et al., 2024a)	AR	82.33	87.38	87.70	85.46	86.41	79.68
Janus-Pro (Chen et al., 2025c)	AR	87.58	88.63	88.17	88.98	88.30	82.63
BLIP-3o (Chen et al., 2025a)	AR+Diff.	-	-	-	-	-	81.60
Tar (Han et al., 2025)	AR	83.59	89.35	86.91	93.50	80.80	82.96
MMaDA (Han et al., 2025)	Discrete Diff.	77.81	78.48	81.74	84.79	63.20	69.97
FUDOKI (Wang et al., 2025)	DFM	80.55	89.73	88.05	93.66	78.00	83.63
NExT-OMNI	DFM	81.09	89.76	88.36	94.37	81.63	84.46

Table 13: **Comparison with state-of-the-art methods on speech-language and audio-language benchmarks.** Here, “T”, “S”, and “A” represent text, speech (belonging to the audio modality) audio inputs, respectively.

Model	Librispeech (EN-WER)				AudioCaps	
	Test_clean		Test_other		Test	
	S→T	T→S	S→T	T→S	A→T	T→A
Speech Only						
SpeechT5 (Ao et al., 2021)	2.4	-	5.8	-	-	-
SALMONN (Sun et al., 2024a)	2.1	-	4.9	-	-	-
Mini-Omni (Xie & Wu, 2024)	4.7	-	9.4	-	-	-
Freeze-Omni (Wang et al., 2024c)	3.2	-	7.7	-	-	-
Qwen2-Audio (Chu et al., 2023)	2.0	-	4.5	-	-	-
Omnimodal Und.						
VITA (Fu et al., 2024)	8.1	-	18.4	-	-	-
EMOVA (Chen et al., 2024b)	4.0	3.4	-	-	-	-
VITA 1.5 (Fu et al., 2024)	3.4	-	7.5	-	-	-
OpenOmni (Luo et al., 2025)	3.1	3.4	7.0	7.8	-	-
Stream-Omni (Zhang et al., 2025a)	3.0	-	7.2	-	-	-
Omnimodal Und. and Gen.						
AnyGPT (Zhan et al., 2024)	8.5	-	-	-	-	-
UnifiedIO2-xxlarge (Lu et al., 2024)	-	-	-	-	48.9	2.64
OmniFlow (Li et al., 2025c)	-	-	-	-	78.4	1.75
NExT-GPT (Wu et al., 2023)	-	-	-	-	81.3	1.74
NExT-OMNI	3.0	3.1	7.0	7.2	84.8	1.65

Table 14: **Comparison with state-of-the-art methods on the video understanding benchmarks**.

Model	MSVD-QA	MSRVTT-QA	TGIF-QA	ActivityNet-QA
Und. Only				
Video-Chat (Li et al., 2023a)	56.3	45.4	34.4	-
VideoLLaMA (Zhang et al., 2023b)	51.6	29.6	-	-
Video-ChatGPT (Maaz et al., 2023)	64.9	49.3	51.4	35.2
Video-LLava (Lin et al., 2023)	70.7	59.2	70.0	45.3
Und. and Gen.				
UnifiedIO2 (Lu et al., 2024)	52.1	42.5	-	-
NExT-GPT (Wu et al., 2023)	64.5	61.4	-	-
Emu (Sun et al., 2023)	-	18.8	8.3	-
Emu2 (Sun et al., 2024b)	31.4	28.7	-	-
SEED-LLaMA (Ge et al., 2023b)	40.9	30.8	-	-
VILA-U (Wu et al., 2024c)	73.4	58.9	51.3	51.6
NExT-OMNI	76.2	62.7	58.1	56.4

Table 15: **Comparison with state-of-the-art methods on video generation benchmarks VBench (Huang et al., 2024).**

Model	Total Score	Quality Score	Semantic Score
Open-Sora (OpenAI, 2025)	75.9	78.8	62.3
CogVideo (Hong et al., 2022)	67.0	72.1	46.8
VILA-U (Wu et al., 2024c)	74.0	76.3	65.0
NExT-OMNI	80.1	80.8	77.5

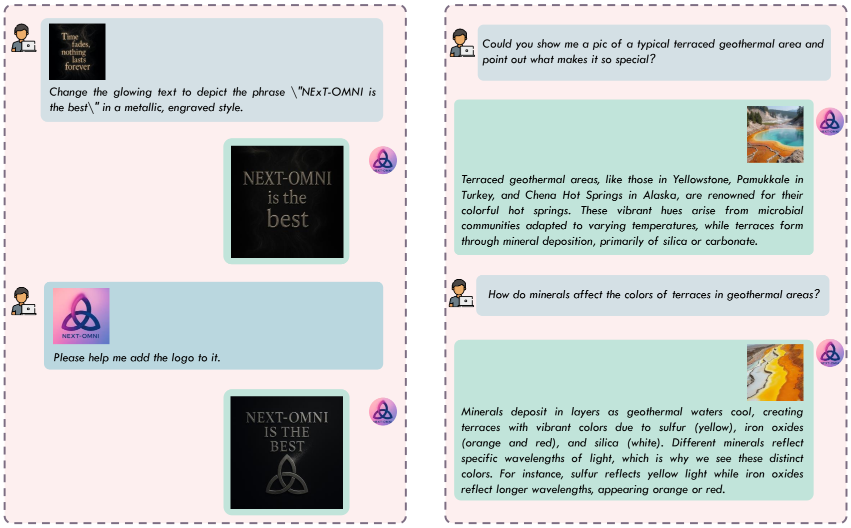

Change the glowing text to depict the phrase \"NExT-OMNI is the best\" in a metallic, engraved style.

Please help me add the logo to it.

Could you show me a pic of a typical terraced geothermal area and point out what makes it so special?

Terraced geothermal areas, like those in Yellowstone, Pamukkale in Turkey, and Chena Hot Springs in Alaska, are renowned for their colorful hot springs. These vibrant hues arise from microbial communities adapted to varying temperatures, while terraces form through mineral deposition, primarily of silica or carbonate.

How do minerals affect the colors of terraces in geothermal areas?

Minerals deposit in layers as geothermal waters cool, creating terraces with vibrant colors due to sulfur (yellow), iron oxides (orange and red), and silica (white). Different minerals reflect specific wavelengths of light, which is why we see these distinct colors. For instance, sulfur reflects yellow light while iron oxides reflect longer wavelengths, appearing orange or red.

Figure 8: **Visualization case of multi-turn vision-language interaction.**

I Additional Visualization

In addition to the above experimental results, we provide additional visualization cases to supplement the demonstration of NExT-OMNI's extensive application scenarios and interesting properties.

Interesting Properties. We demonstrate NExT-OMNI's iterative refinement inference process across different modal data in Figure 11. Figure 16 presents image generation quality comparisons with other similar models. Figure 21 showcases zero-shot cross-modal generalizability, capable of accepting arbitrary data inputs and generating relevant outputs in other modalities. Figure 13 illustrates discrete flow matching's single forward pass extraction of unified representations for cross-modal retrieval. Moreover, as shown in Figure 22, NExT-OMNI can spontaneously perform "think with images" without relying on external tools. By unlocking image generation during the reasoning process, it can better solve complex tasks and improve performance, demonstrating the considerable potential of NExT-OMNI.

High-Level Multi-Turn Interaction. We demonstrate multi-turn visual interaction capabilities in Figure 8, where the model can autonomously perceive and select appropriate positions for image generation, or manually control image generation positions. Figure 9 showcases multi-turn speech interaction capabilities, where the model can accept speech inputs and produce speech outputs.

Basic Single-Turn Interaction. We also supplement visualization cases of NExT-OMNI's single-turn interactions, including image generation in Figure 14, audio generation in Figure 15, video generation in Figure 17, and omnimodal understanding in Figure 10, image understanding in Figure 18, audio understanding in Figure 19, and video understanding in Figure 20. Overall, NExT-OMNI can accomplish fundamental single-turn multimodal interactions with strong capabilities.

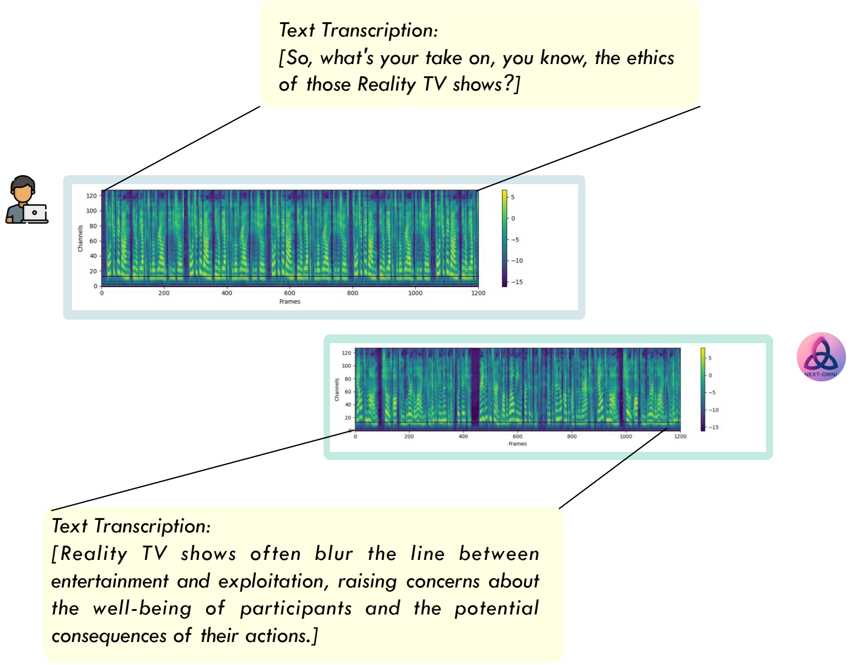

Text Transcription:
[So, what's your take on, you know, the ethics of those Reality TV shows?]

Text Transcription:
[Reality TV shows often blur the line between entertainment and exploitation, raising concerns about the well-being of participants and the potential consequences of their actions.]

Figure 9: **Visualization case of multi-turn speech-language interaction.**

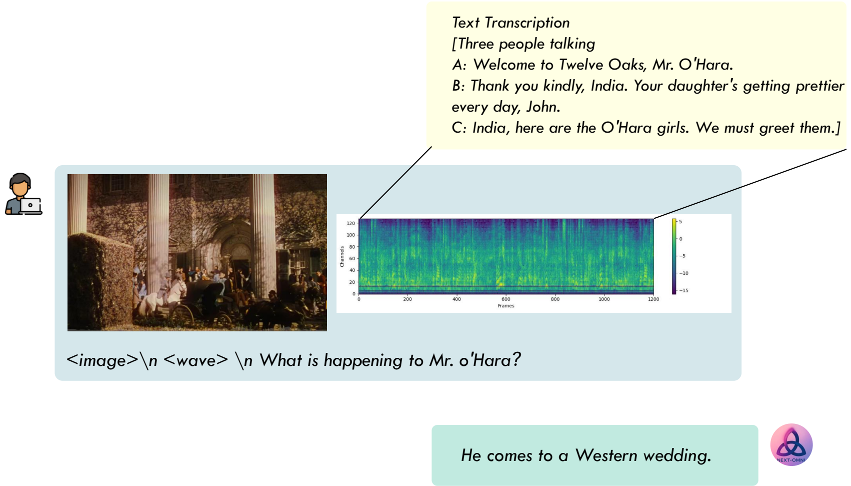

Text Transcription
[Three people talking
A: Welcome to Twelve Oaks, Mr. O'Hara.
B: Thank you kindly, India. Your daughter's getting prettier every day, John.
C: India, here are the O'Hara girls. We must greet them.]

<image>\n <wave> \n What is happening to Mr. o'Hara?

He comes to a Western wedding.

Figure 10: **Visualization case of omnimodal understanding.**

J The Use of Large Language Models

We declare that large language models (LLMs) were employed to assist with the refinement of this manuscript, specifically, for grammar checking, language polishing, and improving the clarity and fluency of the text. Additionally, LLMs were used in a limited capacity for minor debugging and syntactic correction of code snippets included in the work.

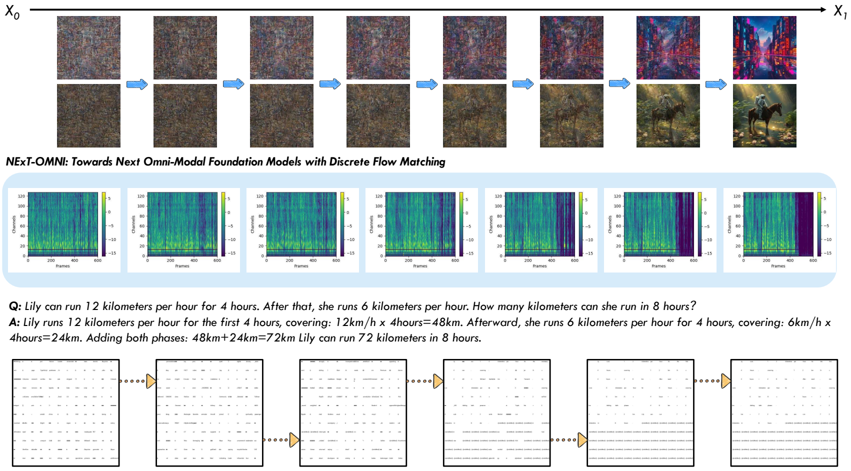

NExT-OMNI: Towards Next Omni-Modal Foundation Models with Discrete Flow Matching

Q: Lily can run 12 kilometers per hour for 4 hours. After that, she runs 6 kilometers per hour. How many kilometers can she run in 8 hours?
A: Lily runs 12 kilometers per hour for the first 4 hours, covering: 12km/h x 4hours=48km. Afterward, she runs 6 kilometers per hour for 4 hours, covering: 6km/h x 4hours=24km. Adding both phases: 48km+24km=72km Lily can run 72 kilometers in 8 hours.

Figure 11: **Visualization case of iterative refinement process.**

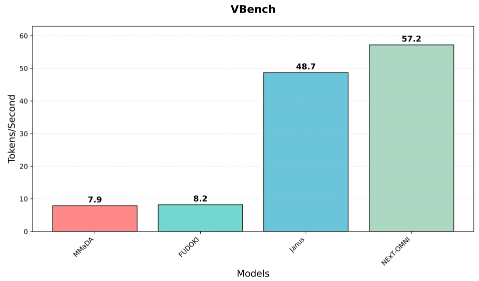

Figure 12: **Visualization case of speed comparison on VBench (Huang et al., 2024).**

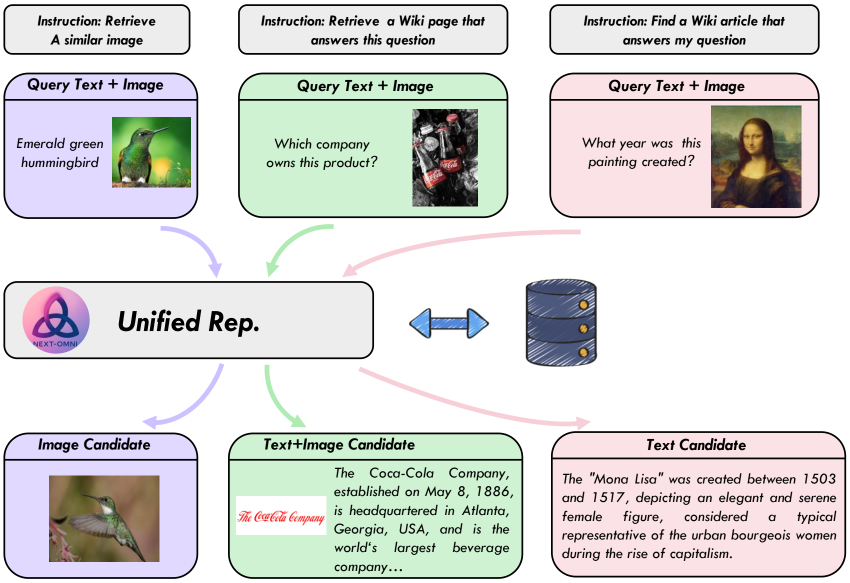
Instruction: Retrieve A similar image
Instruction: Retrieve a Wiki page that answers this question
Instruction: Find a Wiki article that answers my question
Query Text + Image
Query Text + Image
Query Text + Image
Unified Rep.
NEXT-OMNI
Image Candidate
Text+Image Candidate
Text Candidate
The Coca-Cola Company

Emerald green hummingbird

Which company owns this product?

What year was this painting created?

The Coca-Cola Company, established on May 8, 1886, is headquartered in Atlanta, Georgia, USA, and is the world's largest beverage company…

The "Mona Lisa" was created between 1503 and 1517, depicting an elegant and serene female figure, considered a typical representative of the urban bourgeois women during the rise of capitalism.

Figure 13: **Visualization case of multimodal retrieval based on unified representation.**

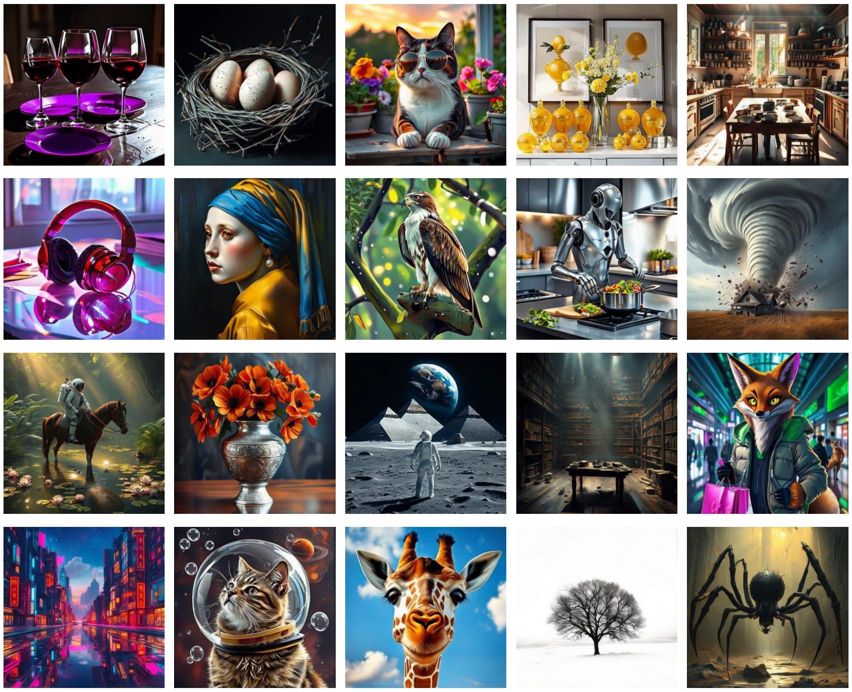

Figure 14: **Visualization case of image generation.**

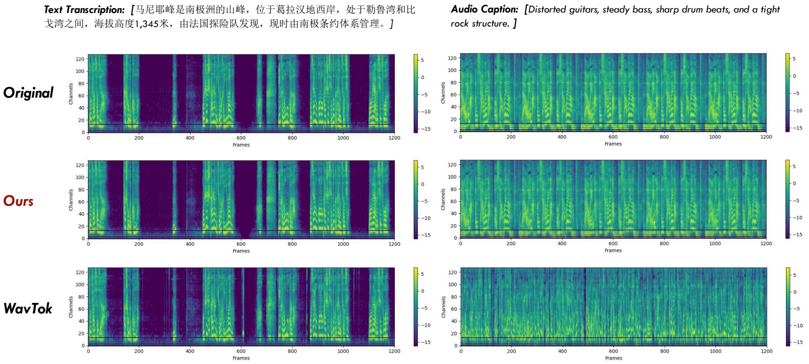

Figure 15: **Visualization case of audio generation.**

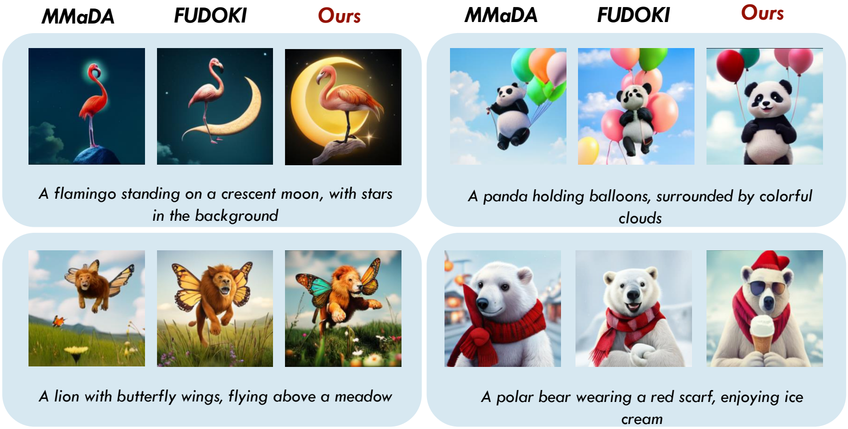
MMaDA
FUDOKI
Ours
MMaDA
FUDOKI
Ours
A flamingo standing on a crescent moon, with stars in the background
A panda holding balloons, surrounded by colorful clouds
A lion with butterfly wings, flying above a meadow
A polar bear wearing a red scarf, enjoying ice cream

Figure 16: **Visualization case of image quality comparison.**

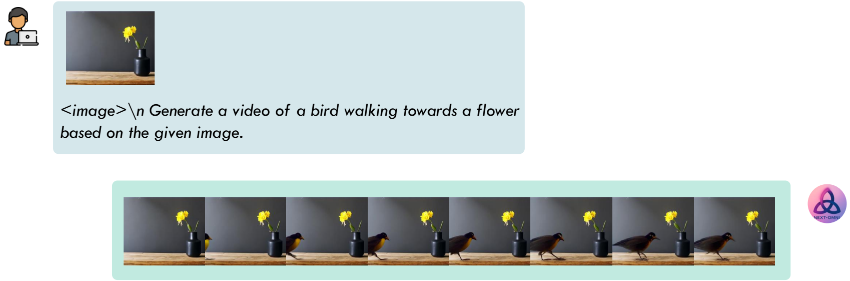

<image>\n Generate a video of a bird walking towards a flower based on the given image.

Figure 17: **Visualization case of video generation.**

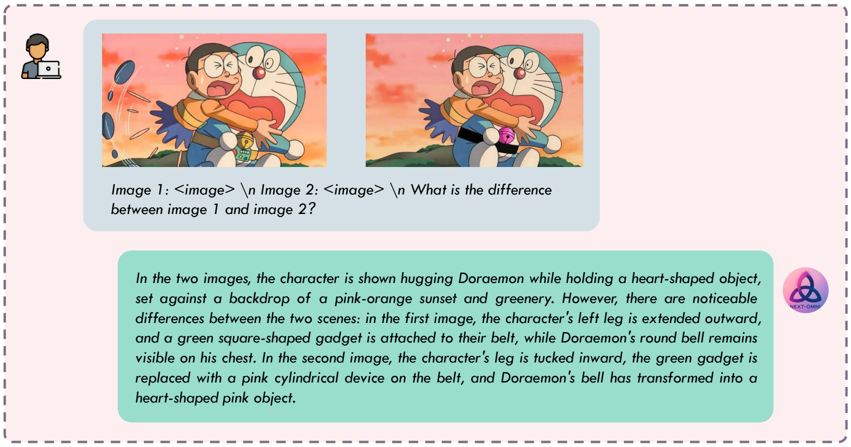

Image 1: <image> \n Image 2: <image> \n What is the difference between image 1 and image 2?

In the two images, the character is shown hugging Doraemon while holding a heart-shaped object, set against a backdrop of a pink-orange sunset and greenery. However, there are noticeable differences between the two scenes: in the first image, the character's left leg is extended outward, and a green square-shaped gadget is attached to their belt, while Doraemon's round bell remains visible on his chest. In the second image, the character's leg is tucked inward, the green gadget is replaced with a pink cylindrical device on the belt, and Doraemon's bell has transformed into a heart-shaped pink object.

Figure 18: **Visualization case of image understanding.**

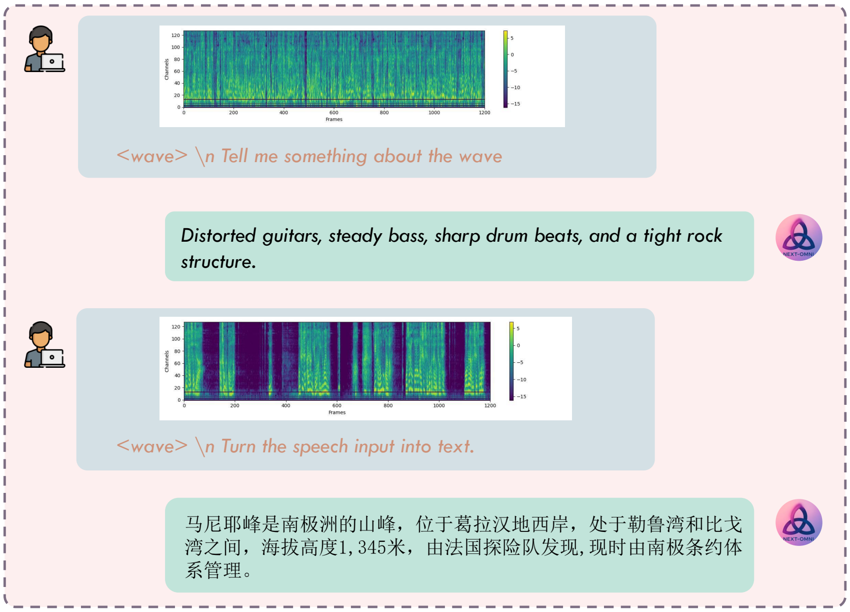

<wave> \n Tell me something about the wave

Distorted guitars, steady bass, sharp drum beats, and a tight rock structure.

<wave> \n Turn the speech input into text.

马尼耶峰是南极洲的山峰，位于葛拉汉地西岸，处于勒鲁湾和比戈湾之间，海拔高度1,345米，由法国探险队发现,现时由南极条约体系管理。

Figure 19: **Visualization case of audio understanding.**

<image><image><image><image><image><image><image><image>\n Elaborate on the visual and narrative elements of the video in detail.

The video shows a close-up of a large pile of meat, likely chicken, being cooked on a grill. The meat is covered in a red sauce, possibly a marinade or a barbecue sauce. The grill is outdoors, as indicated by the blurred greenery in the background. The meat is being cooked in a large pan or tray, which is placed on the grill. The cooking process is shown in three stages: the meat is first placed on the grill, then it is covered with the red sauce, and finally, it is cooked until it reaches a golden-brown color. The style of the video is realistic and it captures the details of the cooking process.

Figure 20: **Visualization case of video understanding.**

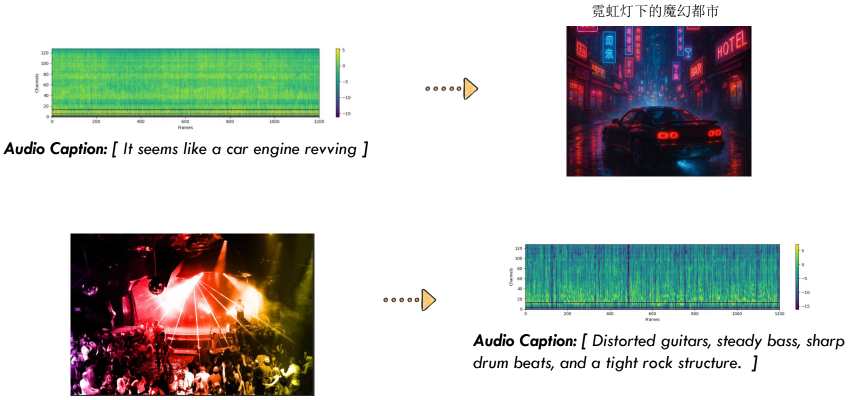

Audio Caption: *[It seems like a car engine revving]*

Audio Caption: *[Distorted guitars, steady bass, sharp drum beats, and a tight rock structure.]*

Figure 21: **Visualization case of cross-modal generation.**

(Think with Image). Fruit Grid Puzzle

The fruit plate is a 2×2 grid, with each cell containing a fruit. The initial state is as follows:
Apple Banana
Pear Orange

Step 1: Swap the positions of the fruit in the top-left corner (cell 1) and the fruit in the bottom-right corner (cell 4).

Step 2: Rearrange the fruits according to the following rules:
• If the fruit is round, it must be placed in the upper part of the grid.
• All other non-round fruits must be placed in the lower part of the grid.

Step 3: Rotate the fruit positions **clockwise by one position.**

Output the final fruit plate state with minimum operation cost.

1. First, I present the initial state <image1>.
2. Next, we swap the top-left and bottom-right fruits <image2>.
3. Then we rearrange according to the rules (round fruits above, non-round fruits below) <image3>.
4. Wait, it appears that the round fruits are apple and orange, while the non-round fruits are . banana and pear. I made an error. Now rearranging according to the rules <image4>.
5. It seems this doesn't satisfy the minimum operation cost requirement and needs correction <image5>.
6. Rotate the fruit positions clockwise by one position <image6>.

****Final Answer:****
Pear Orange
Banana Apple ✓

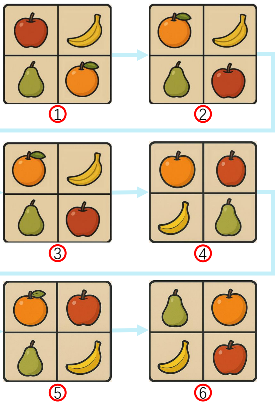

Figure 22: **Visualization case of thinking with images.** NExT-OMNI can enhance its reasoning ability through the 'thinking with images' mode, demonstrating strong potential in integrating visual cues into intermediate reasoning steps, which improves interpretability and enables more accurate problem-solving across complex multimodal tasks.